COPPER FERRITE SYNTHESIS FROM EXTRACTION OF CHALCOPYRITE AND INVESTIGATION OF ITS ELECTROCHEMICAL PROPERTIES

2022
MASTER THESIS
METALLURGY AND MATERIALS ENGINEERING

MARIEM MOHAMED EL MAMY

Thesis Advisor
Assist. Prof. Dr. Safa POLAT

COPPER FERRITE SYNTHESIS FROM EXTRACTION OF CHALCOPYRITE AND INVESTIGATION OF ITS ELECTROCHEMICAL PROPERTIES

MARIEM MOHAMED EL MAMY

T.C.
Karabuk University
Institute of Graduate Programs
Department of Metallurgy and Materials Engineering
Prepared as
Master Thesis

Thesis Advisor

Assist. Prof. Dr. Safa POLAT

KARABUK

September 2022

I certify that in my opinion the thesis submitted by Mariem Mohamed EL MAMY titled "COPPER FERRITE SYNTHESIS FROM EXTRACTION OF CHALCOPYRITE AND INVESTIGATION OF ITS ELECTROCHEMICAL PROPERTIES" is fully adequate in scope and in quality as a thesis for the degree of Master of Science.

Assist. Prof. Dr. Safa POLAT .....
Thesis Advisor, Department of Metallurgy and Materials Engineering

This thesis is accepted by the examining committee with a unanimous vote in the Department of Metallurgy and Materials Engineering as a Master of Science thesis. September 29, 2022

Examining Committee Members (Institutions)	Signature
Chairman : Assoc. Dr. Yüksel AKINAY (YYU)	Online
Member : Assist. Prof. Dr. Safa POLAT (KBU)	.....
Member : Assist. Prof. Dr. Alper İNCESU (KBU)	.....

The degree of Master of Science by the thesis submitted is approved by the Administrative Board of the Institute of Graduate Programs, Karabuk University.

Prof. Dr. Hasan SOLMAZ .....
Director of the Institute of Graduate Programs

"I declare that all the information within this thesis has been gathered and presented in accordance with academic regulations and ethical principles and I have according to the requirements of these regulations and principles cited all those which do not originate in this work as well."

Mariem Mohamed El Mamy

ABSTRACT

M. Sc. Thesis

COPPER FERRITE SYNTHESIS FROM CHALCOPYRITE AND INVESTIGATION OF ITS ELECTROCHEMICAL PROPERTIES

Mariem Mohamed EL MAMY

Karabuk University
Institute of Graduate Programs
Department of Metallurgy and Materials Engineering

Thesis Advisor:
Assist. Prof. Dr. Safa POLAT
September 2022, 63 pages

This thesis study consists of two stages, extraction and electrode production. In the first stage, the effects of NaCl, $MgCl_2$, and Urea compounds on the extraction of Cu and Fe from chalcopyrite ore were investigated. For this purpose, different ratios of these compounds were added to the extraction solution, and then each solution's Cu and Fe concentrations were measured. Measurements were performed by atomic absorption spectroscopy (AAS). According to the obtained results, the concentration of Cu and Fe increased by 76% and 28%, respectively, with the addition of NaCl and approximately 52% and 53% with the addition of $MgCl_2$. At the same time, when $MgCl_2$ and Urea were added together, these values decreased by 12% and 35%. The second stage is aimed at producing nano-sized copper ferrite-based electrodes from the obtained solutions. The productions were carried out directly on the nickel foam surface by hydrothermal method. The produced electrodes were characterized by

FTIR, XRD, and SEM in terms of chemical bond structures, crystal planes, and microstructures, respectively. In addition, the electrochemical performance of the produced electrode was investigated by galvanostatic charge-discharge measurements (GCD) with a three-electrode system. From these examinations, firstly, the specific capacitance values (Ca) and then the energy (E) and power density (P) values were determined. Based on these results, the highest Ca value was determined as 725 mF/cm^2 at 2 mA current, while E and P values were calculated as approximately 12.5 mWh/cm^2 and 880 mW/cm^2. In addition, these results were compared and discussed with the studies done so far. Finally, it was concluded that the extraction of Cu and Fe from chalcopyrite with a very cheap compound such as NaCl could be performed at higher rates than their literature counterparts. Furthermore, a very high-performance electrode for supercapacitors, an important component of energy storage systems, has been produced with the obtained solutions. It is also thought that the electrochemical performances of these electrodes are promising for supercapacitors but should be investigated in more detail for this purpose.

Key Words : Chalcopyrite, extraction, nanoparticle, metal oxide, hydrothermal method, supercapacitor.

Science Code : 91520, 91530

ÖZET

Yüksek Lisans Tezi

KALKOPİRİTTEN BAKIR FERRİT SENTEZİ VE ELEKTROKİMYASAL ÖZELLİĞİNİN İNCELENMESİ

Mariem Mohamed EL MAMY

Karabük Üniversitesi
Lisansüstü Eğitim Enstitüsü
Metalurji ve Malzeme Mühendisliği Anabilim Dalı

Tez Danışmanı:
Dr. Öğr. Üyesi Safa POLAT
Eylül 2022, 63 sayfa

Bu tez çalışması ekstraksiyon ve elektrot üretimi olmak üzere iki aşamadan oluşmaktadır. İlk aşamada kalkopirit cevherinden Cu ve Fe ekstraksiyonuna NaCl, $MgCl_2$ ve Üre bileşiklerinin etkileri incelenmiştir. Bu amaçla ekstraksiyon solüsyonuna bu bileşiklerden farklı oranlarda eklenmiş ve daha sonra her bir solüsyonun Cu ve Fe konsantrasyonları ölçülmüştür. Ölçümler atomik absorpsiyon spektroskopisi (AAS) ile gerçekleştirilmiştir. Elde edilen sonuçlara göre Cu ve Fe konsantrasyonu NaCl eklentisi ile sırasıyla %76 ve %28 oranlarında, $MgCl_2$ eklentisi ile yaklaşık %52 ve %53 oranlarında artmıştır. Aynı zamanda $MgCl_2$ ve Üre birlikte eklendiğinde ise bu değerler %12 ve %35 olarak oranlarında düşmüştür. İkinci aşamada ise buradan elde edilen solüsyonlardan nano boyutlu bakır ferrit bazlı elektrot üretilmesi amaçlanmıştır. Üretimler hidrotermal yöntemle nikel foam yüzeyinde doğrudan gerçekleştirilmiştir. Elde edilen ürünlerin kimyasal bağ yapıları, kristal düzlemleri ve mikroyapıları sırasıyla FTIR, XRD ve SEM ile karakterize edilmiştir.

Ayrıca üretilen elektrotun elektrokimyasal performansı ise üç elektrotlu sistem ile galvano statik şarj deşarj ölçümleri (GCD) ile incelenmiştir. Bu incelemelerden öncelikle spesifik kapasitans değerleri (Ca) daha sonra ise enerji (E) ve güç yoğunluğu (P) değerleri tespit edilmiştir. Elde edilen sonuçlara göre en yüksek Ca değeri 2 mA akımda 725 mF/cm^2 olarak tespit edilirken, E ve P değerleri ise yaklaşık 12.5 mWh/cm^2 ve 880 mW/cm^2 olarak hesaplanmıştır. Ayrıca elde edilen bu sonuçlar şimdiye kadar yapılmış olan çalışmalar ile tartışılarak kıyaslanmıştır. Nihai olarak kalkopiritten NaCl gibi oldukça ucuz bir bileşik ile Cu ve Fe ekstraksiyonunun literatürdeki muadillerine kıyasla daha yüksek oranlarda gerçekleştirilebildiği sonucuna varılmıştır. Ayrıca elde edilen solüsyonlar ile enerji depolama sistemlerinin önemli bir bileşeni olan süperkapasitörlere yönelik oldukça yüksek performanslı bir elektrot üretimi de gerçekleştirilmiştir. Bu elektrotların elektrokimyasal performanslarının süperkapasitörler için umut vadedici olduğu ancak bu amaçla daha ayrıntılı olarak incelenmesi gerektiği düşünülmektedir.

Anahtar Kelimeler **:** Kalkopirit, ekstraksiyon, nanopartkül, metal oksit, hidrotermal metot, süperkapasitör.

Bilim Kodu **:** 91520, 91530

ACKNOWLEDGMENT

First of all, I want to thank the omnipotent God for the blessings he gave me during my research.

I would like to express my sincere thanks to my advisor Assist. Prof. Dr. Safa Polat. It was a great privilege and honor to work and study under his direction.

I would also like to thank Research Assistant Güldane Ateşoğlu for her help and for giving the chalcopyrite I used in my thesis.

I would like to express my gratitude to the nano energy laboratory team graduate students Muwafaq Mashrah, Mariem Abdi, Moctar Mbebou, and Cheikh Sidi Mohamed Lefdhil, who helped me from using laboratory equipment to writing the thesis while I was doing my experimental work.

I am incredibly grateful to my parent for their love, prayers, caring, and sacrifice in educating me and preparing me for my future. Also, I thank my family, brothers and sisters, friends, and everyone.

I would also like to thank the laboratories of Karabuk University Iron and Steel Institute Materials Research and Development Center (MARGEM) for allowing me to use the laboratory facilities.

I would also like to thank the project numbered KBÜBAP-21-ABP-047 of Karabuk University Scientific Research Projects Unit (KBU-BAP), which provided funding for the analyses.

CONTENTS

Page

Page

LIST OF FIGURES

Page

LIST OF TABLES

Page

SYMBOLS AND ABBREVITIONS INDEX

SYMBOLS

A	: Ampere
mA	: Milliampere
µm	: Micrometer
g	: Gram
mg	: Milligram
cm^3	: Centimeter cubic
L	: Liter
°C	: Degrees Celsius
K	: Kelvin
s	: Second
Cu	: Copper
Fe	: Iron
NaCl	: Sodium chloride
$MgCl_2$	: Magnesium chloride
KCl	: Potassium chloride
CaCl	: Calcium chloride
mF	: Millifarad
mWh/cm^2	: Milliwatts hour per centimeter squared
mW/cm^2	: Milliwatts per centimeter squared
$CuFeS_2$	: Chalcopyrite
SO_2	: Sulfur dioxide
CO_2	: Carbon dioxide
Cl	: Chloride
S	: Sulphury

ABBREVITIONS

SEM : Scanning Electron Microscope

XRD : X-Ray Diffraction

XPS : X-ray photoelectron spectroscopy

FTIR : Fourier Transform Infrared Spectroscopy

AAS : Atomic absorption spectroscopy

CFO : Copper ferrite ($CuFe_2O_4$)

CVD : Chemical vapor deposition

PVD : Physical vapor deposition

M : Molar

GCD : Galvanostatic charge-discharge

Ca : Specific capacitance

E : Energy density

P : Power density

g-C_3N_4: Graphitic carbon nitride

GNPs : Graphene nanoplates

PVDF : Polyvinylidene difluoride

PART 1

INTRODUCTION

People meet all their needs from natural resources throughout their lives. The production of almost all of the tools and equipment that makes life functional requires using natural resources. Soil, water, animals, forest, sunlight, petroleum, raw mineral materials, and even the air we breathe can be given as examples of natural resources in every aspect of our lives. If we need to classify these resources in terms of their origins, we can divide them into biotic and abiotic [1]. Natural resources, called biotics, consist of organic substances and living things. Plants, animals, and fossil fuels (such as oil, coal, and natural gas) are also natural resources of organic origin. Abiotic natural resources are natural resources of inorganic (non-living) origin, such as air, water, sunlight, minerals, and metals [2].

Among natural resources, minerals and metals are essential for the socioeconomic development of nations. It also meets energy and industry's basic raw material needs [3]. Therefore, wealth, welfare, and comfortable life for the individual and society are possible with the access and use of mineral raw material resources [4]. These formations, called minerals, were formed by natural factors in the inner and outer parts of the earth's crust and should have economic value [5]. For this reason, it can be said that not every mineral is valuable.

On the other hand, precious minerals are related to the metals commonly used daily. On the other hand, metals are elements with high electrical and thermal conductivity, unique shine, tendency to form, high tendency to form cations, and often give basic oxides by combining with oxygen. Metals can be classified as noble metals (such as gold, silver, and platinum) and non-noble metals (such as iron, zinc, and aluminum) [6,7]. Semi-metals do not show good metal properties. These elements show both

metal and nonmetal properties. Elements such as silicon, boron, antimony, and arsenic are semi-metals [8]. Although nonmetals are more common in nature, most of the elements in the periodic table are metals. Metals daily are iron, aluminum, copper, zinc, magnesium, nickel, tungsten, and mercury [9].

Among metals, copper (Cu) was the first metal to be processed by humans. A stronger bronze was obtained by mixing tin and copper, leading to the beginning of the Bronze Age [10]. Because it conducts heat and electricity very well and can be easily shaped, copper's greatest use is in electrical appliances and wires. However, there is also copper in machinery used in construction and industry. In addition, copper sulfate is used as a pesticide to kill algae in water treatment [11]. Iron (Fe) metal is the fourth most common mineral on the earth's surface and the most abundant metal in the earth's crust [12]. Iron is the most used of all metals and accounts for 95% of the weight of metals produced worldwide. Its low price and high strength properties make it indispensable for use in automotive, ship hull construction, and as a structural component of buildings [13]. On the other hand, steel is an alloy formed by iron with carbon elements, and its mechanical resistance and friction protection is quite high. It is frequently used in kitchenware, sinks, household appliances, industrial kitchens, the food industry, automotive industry [14].

The most widely known copper-iron source is the chalcopyrite mineral. Its composition is $CuFeS_2$, and its density is between 4.1-4.3 g/cm^3. It is also called fake gold because its crystals are brittle, rice yellow in color, and have metallic luster [15]. Obtaining copper and iron from this mineral is carried out by pyrometallurgical and hydrometallurgical methods. In the pyrometallurgical method, a series of heat treatments are applied to the mineral to reveal the precious metal.

In contrast, in the hydrometallurgical method, the metals in the mineral are dissolved and separated with some reagents. Gases such as SO_2 and CO_2 formed due to pyrometallurgical processes cause environmental problems such as air pollution [16]. Although these gases emerging in some enterprises are evaluated, it is a fact that pyrometallurgical processes harm the environment. The hydrometallurgical method must not require high temperatures, low-grade and complex ores can be evaluated,

each metal can be recovered separately and in high purity, and it is economical [17]. For this reason, it can be said that the hydrometallurgical method has an important advantage in its application in producing metals widely used daily, especially copper and iron.

Many successful studies have been carried out on the hydrometallurgical production of copper and iron from chalcopyrite. However, some problems were reported in these studies. These are problems such as the low rate of Cu extraction due to the choice of solvent reactant and the passage of iron into solution along with copper in these extractions. In addition, it was also stated that the sulfur element, which is between the chalcopyrite crystals during the extraction, oxidizes and settles on the chalcopyrite surface, thus preventing the metals from entering the solution. In many studies, acids with high oxygen affinity have been used to solve this passivation problem. However, there is an opinion that with this method, the cost of extraction increases significantly.

For this reason, cheaper chloride sources, which have high redox potential, have a catalytic effect, and can dissolve copper, have been preferred as a reactant. The most common of these is sodium chloride (NaCl), which is very inexpensive and abundant in nature. With this method, $CuCl_2$ and $FeCl_3$ compounds are expected to be formed during the extraction of Cu and Fe from chalcopyrite. In studies conducted for this purpose, it was stated that the extraction by weight of both elements increased significantly with NaCl up to a certain amount. However, these studies concluded that there is still a problem with the passivation layer, and a secondary reactant should be used. The reactant to be used for this purpose must be sulfur-retaining.

On the other hand, it is possible that the oxygen in the urea compound's structure, an organic molecule used as a fertilizer, easily changes with sulfur and turns into thiourea. For this reason, it may be used as a sulfur-absorbing secondary component in such reactions. On the other hand, it is thought that using Cl salts of a magnesium-type component with a high affinity for compounding with oxygen in the environment instead of NaCl may increase the extraction of Cu and Fe.

The coexistence of Cu and Fe elements in the extraction solutions can be considered an important disadvantage, and many methods are applied for their separation. However, this situation can be good thanks to production with both elements. For example, iron and copper elements can form spinel-structured copper ferrite ($CuFe_2O_4$) metal oxide compounds in nature [18]. $CuFe_2O_4$ compound, an important semiconductor, is used in many areas, from cleaning wastewater to microwave absorption, because of its high catalytic, thermal, electrical, and magnetic activities. In recent years, it has been known that metal oxides with spinel structures have also started to be used in energy storage. The most common of these is their use as anode electrode material in supercapacitors. Supercapacitors are devices used to store electro energy. It has the principle of energy storage by absorbing ions or giving redox reactions at the anode and cathode electrodes. For this purpose, since the $CuFe_2O_4$ compound obtained from chalcopyrite can give redox reactions, its energy storage capacity can be quite high. In addition, since ion absorption will affect the energy storage performance, it is very important to synthesize it at the nanoscale. The electrodes of a supercapacitor consist of a conductive current collector and a coating on its surface. The most common current collector used for this purpose is nickel foam. The synthesis of a metal oxide such as $CuFe_2O_4$ on the surface of nickel foam can be carried out by hydrothermal method. The basic principle of this method is to synthesize nano-sized particles from dissolved salts in the liquid phase. The most important advantage is that the synthesis process can be carried out at low temperatures. For this reason, it is possible to synthesize $CuFe_2O_4$ compound on the nickel foam surface by the hydrothermal method in nano size to use it as an anode electrode in supercapacitors.

In light of all these predictions, this thesis study primarily aims to examine the effects of NaCl, $MgCl_2$, and urea compounds in different amounts on the extraction of Cu and Fe from chalcopyrite. For this purpose, Cu and Fe concentrations in the solutions obtained after the extraction processes were measured by atomic absorption, and the results were evaluated. Then, the highest concentration solution was selected, and $CuFe_2O_4$ was synthesized from this solution by hydrothermal method on the nickel foam surface. The obtained products were characterized by FTIR, XRD, and SEM analyses in chemical bonds, crystal structure, and microstructure. Then,

electrochemical characterization was carried out with galvanostatic charge-discharge (GCD) measurements in a three-electrode system to use as a supercapacitor electrode. The results here calculated the produced electrode's specific capacitance, energy, and power densities. Then, the obtained results were compared with the studies in the literature. As a result, information about the advantage, disadvantages, and place of this study in the literature is given.

PART 2

EXTRACTION

2.1. EXTRACTION OF METALS

2.1.1. Pyrometallurgical Methods

Pyrometallurgy is one of the branches of extractive metallurgy. Its primary purpose is to gain precious metals, apply a series of heat treatments to the ore, and cause the material to undergo physical and chemical changes due to these processes. In this way, it is aimed at acquiring precious metals. This method involves drying, calcination, roasting, smelting, and refining. The drying process is applied to remove the material's moisture (not chemically bound). In general, moist solids are dried by the hot gases produced by the combustion of fossil fuels. The heat required in a drying process equals the heat required to evaporate moisture on the solid material. The temperature is usually set above 100 °C, at which water evaporates. The temperature set for this process is usually 105 °C, as the high temperature can also damage the solid material. The purpose of calcination is to remove the water chemically bound to the material. It is made by reducing the material in furnaces at high temperatures. Rotary kilns and fluidized bed reactors are used for this purpose [19].

In the roasting process, the solid material undergoes specific chemical changes under the influence of temperature. During the roasting process, the metal is oxidized. The most typical application of this process can be seen in sulfide metals. Due to their chemical structure, sulfur metals cause problems in advanced refining and blast furnaces. In addition, since the reaction times are long, they increase the energy and time costs. However, with the roasting process, the material reacts by blowing O_2 onto the metal sulfide. While SO_2 gas is formed at the end of the reaction, the metal leaves

the reaction as oxidized. During this process, if all the sulfur in the metal is oxidized, this phenomenon is called "dead roasting" [20].

In some cases, roasting is preferred as a preliminary preparation, and it is undesirable to oxidize all the sulfur in the metal. This type of roasting is also called "partial roasting." In cases where more than two metals are in the environment, one metal oxidizes while the other turns into a sulfate form. This is also called "Selective Roasting." The smelting stage can be defined as the stage in which at least one metal passes into the liquid phase. However, at this stage, the metal is not just melted. However, it undergoes specific chemical reactions. The heat required to carry out this reaction is generally obtained from coal and its derivatives. The oxygen in the metal oxide is reduced with a reducing agent and removed from the metal in the form of CO_2. In other materials, melting of the oxidized ore is facilitated by adding slag makers to the medium. The slag-forming material reacts, and its impurities are removed from the material. Although the melting process usually takes place above the melting temperature of the metal, many variables affect the temperature at which the whole process will be performed. The final stage, refining, is applied to remove the remaining impurities in the metal. However, many processes take place in the refining stage and use more than one different furnace [21].

2.1.2. Hydrometallurgical Methods

Hydrometallurgy is one of the extractive metallurgy methods applied by using liquid chemicals [22]. The primary purpose is to separate, enrich or recycle precious metals from ore. It can be examined under three headings: leaching, purification, and metal recovery. Leaching is the process of recovering precious metals using liquid chemicals with solvent properties. The metal to be enriched is dissolved with chemicals (usually acid or base) and taken into solution. The type and concentration of the selected chemicals may vary according to the properties of the metal to be dissolved. Leaching efficiency can be affected by pH change, temperature, and oxidation potential. As a result of the leaching, along with the metal, other metals present in the ore may have been taken into solution [23].

Specific methods can be used for purification, removing unwanted metals from the solution. Some of these are solvent extraction and ion exchange methods. The primary purpose of solvent extraction is to separate the desired metal by passing it to a different phase. The mixture used in solvent extraction is generally called an organic solvent. The precious metals become organic when the organic solvent is used on the charged solution. As a result, a charged organic and uncharged solution is obtained. The uncharged solution thus obtained can be reused in the process. Electrowinning can separate the charged organic obtained at this stage from the metal [24].

On the other hand, ion exchange is a process in which ions replace ions with similar electrical charges on the solid by attaching to the surface of the solid from a solution in contact with the solid [25]. While these ions on the solid surface pass into the solution, the ions displaced by electrostatic forces bind to the surface and replace them. This exchange process continues until the relative concentrations of the two types of ions on the surface and in the solution reach an equilibrium. The direction of change can be reversed depending on these relative concentrations. The final step in hydrometallurgy is metal recovery. After passing to the liquid phase, the purified metal is recovered by passing it back to the solid phase in this step. The metal obtained after this step can be used as raw material or in further refining processes. For this purpose, electrowinning and metal precipitation methods can be used. In electrowinning, it is applied to reduce the metal due to passing an electric current through the metal-containing solution and its accumulation on the cathode plates. In metal precipitation, it is applied by mixing more active metal (usually Zn) shavings into the solution. While the metal in the sawdust added to the solution passes into the solution, the precious metal is reduced to the solid phase. It begins to accumulate by precipitating on the substrate [26].

2.2. COPPER MINERALS AND CHALCOYRITE

2.2.1. The natural Occurrence of Copper Minerals and Chalcopyrite

Copper ore is found in the earth's crust at an average rate of 0.01% and is the 25th most abundant element. Heavy metal sulfides were decomposed due to liquid infiltration

from the magma layer to the earth's crust. The most common copper mineral, chalcopyrite, $CuFeS_2$ (34.6% Cu), is believed to have formed in this way as a primary (primary). On the other hand, secondary (secondary) oxidized copper minerals and metallic copper (native copper) are also formed due to oxidation and reduction by the chemical effect of hot natural vapors or natural sulfate solutions leaking onto sulfide minerals. For this reason, sulfide copper ores are reached in many mineral deposits as the upper oxidized copper minerals are removed. About 85% of the copper ores known today are sulfide, and 15% are oxide minerals. The most crucial sulfide ores are bornite (Cu_5FeS_4), chalcopyrite ($CuFeS_2$), chalcocite (Cu_2S) and covellite (CuS), and enargite [$Cu_2(As, Sb)S_4$]. Oxidized copper ores, on the other hand, occur as sulfates, carbonates, and silicates. At the same time, azurite [$2CuCO_3 \cdot Cu(OH)_2$], brochantite [$Cu_4SO_4(OH)_6$], chrysocolla [$CuSiO_3 \cdot 2H2O$], cuprite (Cu_2O), tenorite (CuO) and malachite [$CuCO_3 \cdot Cu(OH)_2$] can be given as examples of important oxidized copper ores [27,28].

The chemical formula of the chalcopyrite mineral is $CuFeS_2$, and its molecular weight is 183.53 g. It contains 30.43% Fe, 34.63% Cu, 34.94% S in its composition. It is commonly found in sulfide veins and disseminated volcanic rocks. The crystal system is tetragonal, and the crystal's geometry is shown in Figure 2.1. Fe and Cu can replace Co, Ni, Mn, Zn, Ag, Au, Pb and Cr, and S with Se and Te in this crystal lattice. Thus, chalcopyrite ores may contain many precious metals and nonmetals. Its color is orange-yellowish, its stripe color is greenish-black, its luster is metallic, its density is 4.28 g/cm^3, and its Mohs hardness is 3.5-4 [29–31].

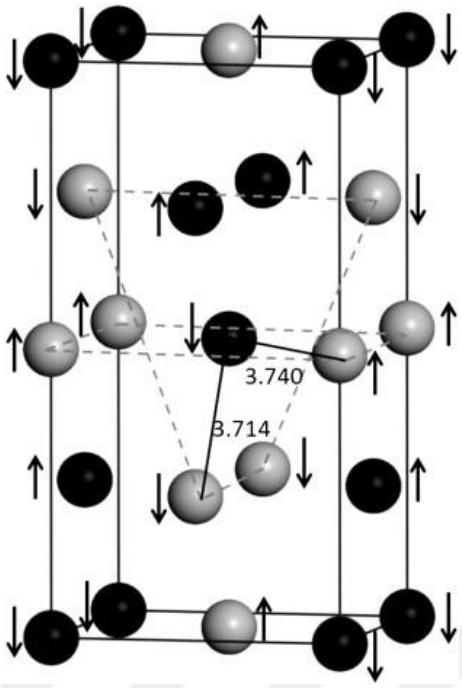

Figure 2.1. Crystal structure of chalcopyrite [29].

2.2.2. Leaching and Dissolution Processes of Chalcopyrite

A leaching process kinetics are especially important for process design, optimization, and control. Kinetic information this type of leaching process can only be obtained through experimentation and observation, and it is influenced by a variety of factors including mineralogy, surface area, reactant concentrations, product layer formation, and temperature [32]. Although many studies have been conducted to establish these factors in the case of chalcopyrite leaching, the results and conclusions have been published in a variety of ways, owing largely to the different conditions used. This has made direct comparisons challenging. In this context, chalcopyrite, which is a sulfide copper ore, can be leached by calcining, or it can be leached directly with suitable solvents. While such calcined products are easily leached with acids or complexing solvents, in case of direct leaching, suitable oxidizing solvents must be used. On the other hand, sulfate, chloride, nitrate, ammonia and biological systems can be used in the leaching of sulfide copper ores [33,34]. Chalcopyrite concentrate can be leached in two steps with sulfuric acid solution. In the first of these, the sulfides in the ore are converted to sulfate with acid at 220-230 °C and then diluted with water and leached

[35]. The reaction steps in this process are given in the Equation 2.1, 2.2, 2.3, and 2.4 below [28].

$$CuFeS_2 + 2H_2SO_4 = CuSO_4 + FeSO_4 + 2H_2S \quad (2.1)$$

$$H_2S + H_2SO_4 = S° + SO_2 + 2H_2O \quad (2.2)$$

$$2FeSO_4 + 2H_2SO_4 = Fe_2(SO_4)_3SO_2 + 2H_2O \quad (2.3)$$

$$CuFeS_2 + 2H_2SO_4 + O_2 = CuSO_4 + FeSO_4 + 2S° + 2H_2O \quad (2.4)$$

On the other hand, chalcopyrite ore can dissolve in the presence of a more dilute solution of sulfuric acid and oxygen. Sometimes ozone is used instead of oxygen. In this context, many hydrometallurgical methods have been developed. The main processes in question can be listed as Cymet, CLEAR, Sherritt Gordon Cominco, H_2SO_4 - pressure in the presence of oxygen and ammonia pressure leaching in the presence of oxygen [36].

The Sherritt Gordon method is the industrial application of leaching sulfide copper minerals with ammonia under pressure [23]. This process is based on the formation of $Cu(NH_3)_4^{+2}$ complex. It was developed to process Ni, Cu, Co complex ore from Lynn Lake mine in Canada. Established facility has been continuing its production since 1954. In this method, concentrated ammonia + ammonium sulfate solution is mixed and leached under oxygen pressure and at a temperature of 85 °C. Some of the free ammonia in the leach solution is separated by distillation. Then, some sulfur compounds in solution are oxidized to sulfate compounds at 250 °C and 27 atm pressure. After neutralizing the free ammonia with sulfuric acid, copper is precipitated with hydrogen at 200 °C under 40 atm pressure and recovered.

The CLEAR (Copper Leaching, Electrowinning and Recycle) process is one of the hydrometallurgical processes using chloride in the processing of chalcopyrite concentrates [37,38]. This process was developed by Duval Corp. It was developed by and includes 2 stages of leaching. In the first stage, chalcopyrite; At boiling

temperature (105 °C) 20 g/L acidic $CuCl_2$ is taken into solution using 4 g/L $FeCl_3$ solution. In the second stage, metallic copper is added to the solution coming from the first stage and the +2-valence copper is converted into Cu^+. Then, solid-liquid separation is made. Copper recovery from the clear solution obtained is carried out by electrolysis method. The leaching sludge is leached in 44 g/L KCl solution at 150 °C temperature and 50 psi oxygen partial pressure in order to dissolve the chalcopyrite that cannot be taken into solution in the first stage. Due to the high temperature and oxygen pressure, some of the sulfur turns into sulfate and precipitates as potassium jarosite ($KFe_3(OH)6(SO_4)_2$). The basic reactions occurring in this context were given below Equation 2.5, 2.6, 2.7, 2.8, and 2.9 [39,40].

$$CuFeS_2 + 3CuCI^+ + 11Cl^- = 4CuCl_3^{-2} + FeCl_2 + S° \quad (2.5)$$

$$Cu + CuCl + 5Cl^- = 2CuCl_3^{-2} \quad (2.6)$$

$$CuFeS_2 + FeCl_2 + 3/2O_2 + 3H_2O = CuCl_2 + 2Fe(OH)_3 + 2S° \quad (2.7)$$

$$CuCl_3^{-2} + e- = Cu^{+3}Cl^- \quad (2.8)$$

$$CuCl_3^{-2} = CuCI^+ + e^- \quad (2.9)$$

$$6FeSO_4 + 12FeCl_2 + 9/2O_2 + 3KCl + 9H_2O = 3KFe_3(SO_4)_2(OH)_6 + 9FeCl_3 \quad (2.10)$$

The Arbiter method is very similar to the Sherritt Gordon method. In the Arbiter method, oxygen is used instead of air and high pressures are not needed. Another difference from the Sherritt Gordon method is that copper is stripped from the solution with the help of ion exchangers [36,41]. Equation 2.11, 2.12, and 2.13 were the dissolutions of different copper minerals in the Arbiter method.

$$CuS + 4NH_3 + 2O_2 = Cu(NH_3)_4SO_4 \quad (2.11)$$

$$Cu_2S + 4NH_3 + (NH_4)_2SO_4 + 5/2\ O_2 = Cu(NH_3)_4SO_4 + H_2O \quad (2.12)$$

$$2CuFeS_2 + 6\ NH_3 + 17/2\ O_2 + (n+2)H_2O$$
$$= 2Cu(NH_3)_4SO_4 + 2(NH_4)_2SO_4 + Fe_2O_3.nH_2O \quad (2.13)$$

2.2.3. Passivation of Chalcopyrite

The majority of copper production from sulfide copper ores and concentrates is done by pyrometallurgical methods. Environmental problems occur due to SO_2 gas output in pyrometallurgical processes. In order to solve this problem, either the cost of the initial investment costs for the sulfuric acid production facility or the difficulties encountered in the storage and marketing of the produced acid have led to the development of alternative hydrometallurgical processes [42].

In leaching processes, the reaction rate shows the variation of the concentration of the reactants or reaction products with time. In leaching processes, the dissolution rate generally decreases with time. This is due to the reduction of the surface area where the reaction takes place, the decrease in solvent concentration or the formation of a protective layer on the surface (passivation) as the reaction time progresses. The dissolution rate also directly depends on the activation energy. The magnitude of the activation energy in the leaching process indicates the difficulty of the dissolution process. In other words, the hardly soluble mineral has high activation energy.

Scientists generally agree that chalcopyrite passivation, or the reduction in the extraction rate of copper from chalcopyrite, occurs as a result of the formation of one or more layers overlying the mineral surface, limiting its reactivity. After many years of research, the nature and extent of these layers' effect on chalcopyrite leaching remain debatable. Some authors attribute this phenomenon to the precipitation of iron oxyhydroxides or jarosites on the mineral surface, which act to cover and isolate it from the solution, causing the leaching process to slow down. Other authors attribute this slowing to the formation of an elemental sulfur layer, which increases in surface area as dissolution progresses, forming a diffusion barrier between the mineral and the leaching medium. Finally, it has been reported that the chalcopyrite dissolution reaction is preceded by the formation of a layer of nonstoichiometric polysulfides or iron-poor sulfides beneath the sulfur layer (which would not cause diffusion issues)

and that this layer reacts slower than the original surface, limiting copper extraction None of these causes has been proven conclusively. The detection of phases such as iron precipitates or polysulfides on sample surfaces, or the coincidence of experimental values with those calculated for diffusion phenomena, has primarily been used to validate their effect on leaching rate. It is likely that more than one of these factors influences overall low-rate chalcopyrite leaching, so it is critical to determine the impact of each on mineral dissolution under the operational conditions used in industrial hydrometallurgy. Dutrizac conducted an early review of some contradictory aspects of chalcopyrite dissolution. There appears to be agreement on two points: particle size affects the process depending on surface area and stirring is only required for particle suspension and gas transfer.

PART 3

NANOPARTICLE AND ENERGY DEPOSITION

3.1. NANOPARTICLE SYNTHESIS

Nanotechnology is the creation of structures with improved and/or completely new physical, chemical and biological properties by working at the level of atoms and molecules (in the range of 1 to 100 nm) in units per billion [43]. In general, the material properties and operating principles of the devices are based on conventional modeling and theory (assumptions based on dimensions greater than 100 nm) [44]. However, when the dimensions are reduced below 100 nm, traditional theories and models are insufficient to explain the emerging features. Compared with large particles of the same materials, nanomaterials exhibit superior and novel properties depending on size. A wide range of nanomaterials or particles can be found naturally on Earth, such as photochemical products, volcanic products, and exhaust fumes. The main purpose of nanotechnology is to develop more robust, better quality, longer life, cheaper, lighter and smaller devices. For this reason, many types of nanoscale production methods are being developed. These are detailed in the section below. In addition, the use and characterization of nanoparticles that can be synthesized for this purpose in supercapacitors are also expressed in the sub-titles [45].

There are two general approaches to the production of nanomaterials and structures: top-down and bottom-up production [46]. In the first approach, called the top-down approach, the process is started with the whole material and the material is divided into small pieces. In this main approach, the structural dimensions of microscopic elements are reduced to the nanometer scale, with lithography, extremely flawless surface shaping, with special processing and chemical etching techniques. In the bottom-up production approach, the material is synthesized as a result of the growth of atoms and molecules in size through chemical reactions [47]. Atomic and molecular elements are

brought together in a controlled manner to form larger systems, clusters, organic lattices, multimolecular structures and synthesized macromolecules. These can be grouped under three groups as solid phase, liquid phase and gas phase synthesis methods [48].

3.1.1. Vapor Phase Synthesis

The inert gas condensation method is a very popular nanoparticle production method because it can provide flexibility and controlled material production [49,50]. The working principle of the method is based on evaporation of the starting material in a clean helium atmosphere and cooling the vapor formed in the helium atmosphere. This process is followed by the condensation of atoms into nano particles and the resulting nano particles are transported and accumulated in the collector. Convection currents (heated by inert gas, cooled by cold finger) carry small, condensed particles into the collection vessel. The deposits are scraped and sent to the compression device. The size of the produced particles is between 1-100 nm and these sizes can be controlled by adjusting the gas pressure. Then, if desired, the collected particles can be sintered to obtain solid nanomaterials. The main parameters affecting the system and the characteristics of the product are gas pressure, type of inert gas, temperature and gas flow rate [51].

Physical Vapor Deposition (PVD) is a method of coating by vapor convection and condensation (usually under vacuum) of material from a solid or liquid source [52]. This method is a versatile production method and thin films can be prepared in atomic or nanometer size, provided that the process conditions are carefully controlled. PVD involves the creation of vapor phase types such as evaporation, sputtering, laser heating or ion beam [53]. In evaporation, atoms are separated from the source by thermal means, in sputtering, they are separated from the target surface by the impact of ions. After the resulting vapor phase passes through the collision and ionization phases, the substrate concentrates on the sample, followed by nucleation and growth processes. In addition, sputtering is used to form layers of materials with high melting points, such as refractory metals and ceramics, which are very difficult to manufacture by thermal evaporation. Sputter-formed films generally have a higher density, as

sputtering atoms carry more energy than evaporating atoms. The major advantages of PVD processes are their high film growth rates and the ability to form dense films at relatively low substrate temperatures [54].

The chemical vapor deposition method (CVC) was first developed in Germany in 1994 and is an ideal method for the production of large quantities of nanoparticles [55]. The method is basically based on the transformation of gaseous material into particles by thermal cracking. CVD is a frequently used material manufacturing technology at nanoscale. Among its applications, it is mostly used for thin film coating on the surface, but it is also used in the production of high purity bulk materials and powders [56]. In the CVD process, gaseous or vaporous raw materials are transported onto the hot substrate and/or chemical reactions take place on the substrate. Reactions occur on or near hot surfaces and solid products are deposited as thin films on the surface. It is possible to synthesize a wide variety of materials with this method. The reactors used in the CVD process are very diverse. They are divided into groups such as hot-walled, cold-walled, low-pressure/atmospheric pressure/high-pressure reactors with or without carrier gas. In these reactors, deposition processes can be performed at temperatures between 473 and 1873 K. At the same time, CVD processes can be divided into different groups in terms of the energy source (plasma, photon, laser, hot filament) used. The CVD process has many advantages. One of the most important advantages is that it usually forms a homogeneous thick film or coating layer on complex shaped parts. Another advantage of the CVD process is that it allows the synthesis of very high purity materials. Other advantages are relatively high deposition rates and generally do not require as high a vacuum as the PVD method [57,58].

3.1.2. Liquid Phase Synthesis

The particle formation mechanism in liquid phase synthesis is the same as in the vapor phase process. Although grain size and crystal shape are not easy to control in typical gas condensation, these properties can be kept under control by using growth-limiting organic ligands in sol-gel and solvothermal syntheses. In chemical precipitation (CP) reactions, nucleation, growth and/or agglomeration processes occur simultaneously. Insoluble particles are usually formed under supersaturation conditions. Nucleation is

the key stage, during which a large number of small particles are formed. On the other hand, secondary processes such as maturation or aggregation significantly affect the size, morphology and properties of the product obtained. In order to facilitate precipitation, supersaturation (saturation), which usually occurs as a result of a chemical reaction, is required. Typical chemical precipitation methods include the production of metals (from aqueous solutions, reduction from non-aqueous solutions, electrochemical reduction, and degradation of metal-organic precursors), oxides (from aqueous and non-aqueous solutions), and metal precursors (by reactions of molecular precursors). In addition, microwave/sonication chemical precipitation processes can also be applied [59,60].

The sol-gel process is also a wet-chemical technique. In this process, a net structure (gel) is produced using a chemical solution (solute solution) or colloidal particles (sol for nanoscale particles) [61]. In the process, a stable sol containing solid particles in solution is first prepared and subsequently gelled by a polycondensation or politzerization reaction. The gel is dried to remove the liquid phase it contains. In the last step, high temperature is applied for the densification (densification) and decomposition of the gels, during which the gel precipitates in the form of pores in the network structure and residual organic contaminants are removed [62]. Sol is a colloidal suspension of solid particles in a liquid phase, while gel is the interconnected network formed between phases. Both reactions yield polymeric sols (without oxide particles larger than 1 nm) instead of particulate metallic sols. Both reactions are multi-step processes and occur sequentially. Sol-gel precursors can be metal alkoxides or inorganic and organic salts. Various studies are carried out with metal (Si, Ti, Zr, Al, B) alkoxide precursors [63,64].

One of the best methods used to produce pure metal oxide nanoparticles is hydrothermal synthesis. With this method, substances that are insoluble at normal temperature and pressure are grown with heterogeneous reaction under high temperature and high-pressure conditions. Crystal growth is carried out in an apparatus consisting of a steel pressure vessel called an autoclave, where the nutrients are contained with the water. Materials that cannot be produced by solid state reaction can be synthesized via hydrothermal synthesis. The final product is obtained, which tends

to have a low melting point, high vapor pressure and thermal decomposition. Intermediate state, meta-stable state and specific phase products can be easily produced, new meta-stable state and other certain condensed state compounds can be synthesized. The most important disadvantages of hydrothermal synthesis are the need for expensive autoclaves, safety problems in the reaction process and the impossibility of observing the reaction process [65,66].

3.1.3. Solid Phase Synthesis

Mechanical Grinding: Mechanical etching is a typical example of a 'top-down' method in the synthesis of Nanomaterials. In this method, the nanomaterial is not prepared from clusters, but by the structural degradation of coarse-particles formed as a result of plastic deformation. Mechanical grinding is simple, requires no expensive equipment, and is a very popular method for obtaining all grades of materials, as well as nanocrystalline materials. In practice, it is important to pay attention to the contamination that may come from the grinding environment or atmosphere and the consolidation of the powder product, nanocrystalline microstructure without coarsening. High-energy mixers, spherical balls, or tumbler mills are used in mechanical grinding. Depending on the number of balls, rotational speed, size, ball/powder mass, grinding time, and the atmosphere in which grinding takes place, energy transfer occurs from the refractor or balls to the powder material. This synthesis method is suitable for the production of amorphous or nano-crystalline alloy particles, elemental or compound powders [47,67].

3.2. ENERGY DEPOSITION SYSTEM AND SUPERCAPACITORS

Increasing fuel costs, pollution, global warming and geopolitical concerns have been among the important problems of modern societies related to their dependence on fossil fuels from past to present [68]. In order to reduce these problems in the global context, the development of other energy sources and storage technologies has been among the important targets of the countries. In this context, many studies have been carried out to develop clean energy sources such as wind, solar, biomass, hydrogen, geothermal and hydrothermal energy [69]. In fact, the electrical energies obtained from

these studies are widely used in many areas of our daily life. However, such sources actually convert kinetic energy into electricity thanks to motion in nature and do not have a stable power output. For this reason, it is very important not only to obtain energy, but also to store it and make it available with appropriate outputs when needed. In this context, devices called capacitors have been used so far to store energy. These are devices obtained by placing an insulating material between two conductive plates. In this system, when a source voltage is applied between two plates of a capacitor, current wants to flow through the insulating material, but the insulating material opposes the electron flow. This resistance phenomenon makes the change creating an effect to store the energy in the dielectric material in the form of electrostatic field. Thus, electricity is stored by loading the plates with an opposite and equal electric charge relative to each other. Its capacitance value directly depends on the dielectric constant of the material between the plates thickness [70]. Based on this information, high capacitance value can be obtained by placing components with high dielectric constant between metal plates theoretically. In this context, it has been reported in the literature that components with perovskite structure and high dielectric constant, such as $BaTiO_3$, $SrTiO_3$, provide very high capacitance [71,72]. Apart from these, polymers such as polyaniline, PVDF and metal oxides have also been used in many electronic devices due to their high capacitance value [73]. However, for recently developed devices, higher performance is needed not only in terms of power but also in terms of energy density and the cyclic charge-discharge time associated with it. Helmholtz thought that higher energy storage capacity could actually be achieved by reducing the thickness of the dielectric material between the plates and expanding the surface area, rather than using materials with high dielectric constant [74]. For this purpose, double-layer supercapacitors have been developed using a conductor with a larger surface area of the dielectric material, a liquid electrolyte for ion exchange, and a separator that allows ions to pass (Figure 3. 1) [75]. During the charging of such a supercapacitor, oppositely charged ions in the electrolyte accumulate at the electrodes. Meanwhile, the thickness of the dielectric material at the interface is actually the size of the ions in the electrolyte (1 nm). In conventional capacitors, this thickness can only be reduced to a maximum of 2-5 μm. Even when only the thickness value is taken into account, almost a thousand times higher capacitance can be obtained. Therefore, the amount of energy that supercapacitors can store is higher than conventional ones.

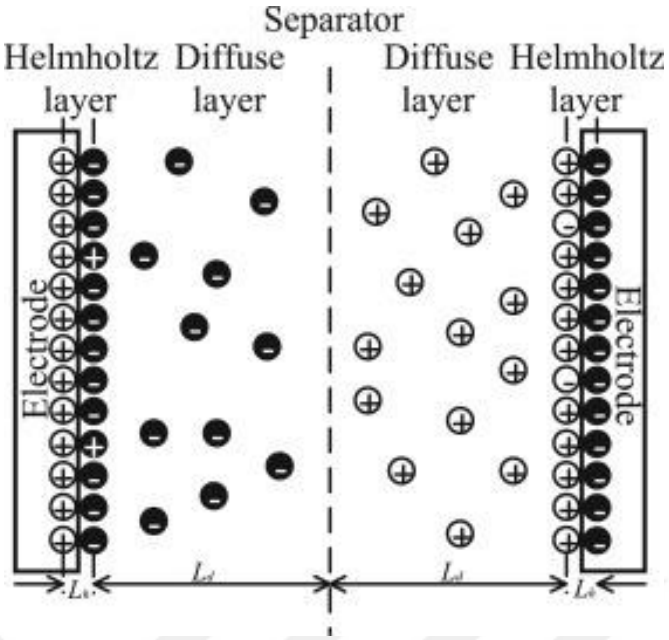

Figure 3.1. Schematic representation of porous supercapacitor electrode [76].

In such supercapacitors, charges on the surface and near the surface can be stored by adsorption or by faradic processes by creating redox reactions on the surface. These are called pseudocapacitors [77]. There are also hybrid ones available in supercapacitors, in which both double-layer and pseudocapacitive type of storage can occur at the same time. In this context, supercapacitors, often called ultracapacitors or electrochemical capacitors, have outstanding power performance, excellent reversibility, very long cycle life (> 1000000 cycles), simple operating mode and integration into electronics. They also generate less thermochemical heat due to simple charge storage mechanisms [78]. For this reason, it has been widely used in consumer electronics, memory backup systems, and industrial power and energy management. Today, it is intended to be used in various energy storage systems such as large industrial machines, electric vehicles and portable electronic devices. Especially for electric vehicles, supercapacitors are expected to have higher energy storage capacity and power density, as well as ultra-superior features that can withstand long cycles and have easy charge-discharge cycles. In order to meet these specifications, all parameters should be developed together, not a single parameter. For example, it is necessary to improve the properties of the collector used as electrode material, such as increasing the energy density by being porous and having a larger surface area, at the same time using a dielectric material that can withstand long cycles and being able to be charged-

discharged fast by performing faradic reactions on this dielectric at the same time. In the literature, many new generation components are being developed in addition to traditional components for this purpose. The most important expectation from these components is that the surface area is large, and the conductivity is high. Metal oxides with spinel structure have higher electrical conductivity compared to other metal oxides in terms of conductivity. Generally, the general formula for a spinel is AB_2O_4. Here, A denotes a divalent metal ion (M^{2+}), and B denotes a trivalent metal ion (M^{3+}). In a normal spinel structure, A ions occupy tetrahedral sites and B ions occupy octahedral sites. Spinel ferrites, MFe_2O_4 (here M = Mn, Co, Ni, Zn, Cu etc.) are fascinating materials due to their impressive magnetic, electrical and optical properties as well as their ability to exhibit different redox states and electrochemical stability [79]. $ZnFe_2O_4$ and Co_3O_4 electrodes from MFe_2O_4 and metal oxide categories are known for their non-toxic structure, high surface area, high specific capacitance, normal spinel structure, readily available metal salts, low cost and environmental harmlessness [80]. In addition, $ZnFe_2O_4$ and Co_3O_4 have high theoretical capacities of 2600 F/g and 3560 F/g, respectively [81]. In general, ferrites ($ZnFe_2O_4$) have a wide potential range (0 V - 1.3 V), which affects the improvement in energy storage density.

PART 4

LITERATURE REVIEW

4.1. LEACHING OF CHALCOPYRITE

Deniz et al. investigated the addition of NaCl to the ammonium persulfate-APS (as an oxidant) leaching of chalcopyrite. They stated that metal extraction increased with increasing NaCl concentration, APS concentration, leaching temperature (up to 333 K) and L/S ratio. The formation of an elemental sulfur layer on the particle surface during the oxidative leaching of sulfur minerals has been expressed as the primary problem causing low metal extraction. They determined that the sulfur layer can eliminate the passivation effect and low dissolution problems in the presence of chloride ions. In the experimental results, copper and iron extraction efficiencies were obtained as 75% and 80%, respectively: APS concentration of 250 g/L; NaCl concentration 150 g/L; duration 180 minutes; temperature 333 K; mixing speed 400 rpm; and L/S 250 mL/g [82].

Velasquez et al. stated that agglomeration occurs during the leaching process. In this context, they investigated the effect of adding chloride ions to aggregation and curing time's effect on the chalcopyrite ore's overall leaching process. They used 20, 50 and 70 kg of chlorine per ton in their study and stated that the presence of chloride ions is necessary to improve the leaching kinetics, however, high chloride concentrations are not required under ambient conditions. As a result, they observed that the copper extraction of chalcopyrite ore agglomerated with high concentrations of acid and chloride ions after 20 days of leaching increased up to 60%, and the extraction rate increased as the curing period increased from 15 days to 80 days [83].

Petrovic et al. investigated the leaching of chalcopyrite concentrate in hydrochloric acid with hydrogen peroxide as a triple oxidizing agent. The effects of leaching variables such as stirring speed, solid-liquid ratio, temperature and HCl and H_2O_2 concentrations on metal extraction were investigated. In these experiments, after 80 minutes of reaction, they obtained a maximum final copper extraction of 33% with 3.0 mol/L H_2O_2 in 0.5 mol/L HCl at room temperature. They also noted that copper extraction increased in the first 60 minutes of the reaction, then essentially stopped due to the rapid catalytic decomposition of hydrogen peroxide. On the other hand, the solid/liquid ratio significantly affected the copper extraction, and the highest copper extraction was obtained in the most dilute suspension (i.e. S/L ratio of 1:100) [84].

Many studies have investigated the dissolution kinetics and mechanism of chalcopyrite. Solis et al., on the other hand, claimed that the passivation layer could be removed by adding organic solvents to the extraction solution. For this purpose, chalcopyrite leaching was carried out in an acid solution with different oxidants (H_2O_2, $CuSO_4$ and O_3) at different temperatures in the presence of alcohols such as 2-propanol and methanol. They determined the activation energy as 42 kJ mol^{-1} in copper dissolution with 2-propanol and hydrogen peroxide at 40 °C and stated that this result is also suitable for the shrinking core model. However, its effectiveness started to decrease due to the degradation of peroxide above 40 °C. They observed that methanol stabilized the copper ion and allowed the formation of prohibited (Cu_2S_2-$6Cu_2S$), which is necessary to obtain high copper extraction [85].

Pan et al. also thought that passivation on the chalcopyrite surface is an important problem and that it can be eliminated by bioleaching. In this context, it was stated that the passivation layer was weakened by adding beads and the copper extraction was increased from 50% to 89.9%. These results were confirmed by SEM and XRD analysis of the chalcopyrite surface [86].

Hernandez et al. investigated the acid effect during the leaching of chalcopyrite in an acidic medium. In this context, different leaching solutions were prepared using different acids (H_2SO_4, HCl and HNO_3) with and without seawater. In the leaching process, copper chloride and ferric chloride were added as oxidizers. They prepared

100 g/L solutions and stirred at 400 rpm at 45 °C for 7 days. A maximum of 37.7% copper extraction was obtained in the test using hydrochloric acid in a seawater-based medium and the presence of copper chloride. In the leaching test using sulfuric acid in the presence of sodium chloride and copper chloride in a seawater-based medium, the maximum copper recovery was obtained as 34.2%. In general, copper extraction in leach tests using a seawater-based acidic medium was higher than in a pure water-based leaching medium [87].

Jianming et al. used ferric and cupric chloride in a nitrogen atmosphere at 97 °C to recover copper from chalcopyrite and remove iron by precipitation as hematite. In these parameters, they observed that the copper extraction was 99% and the iron extraction was 90% after 3-4 weeks of leaching. When they reduced the particle size of chalcopyrite from 26 μm to 15, they observed 0.2% and 2% increases in copper and iron extractions, respectively. They also stated that when the Cu(II)+Fe(III) concentration in the leaching solution drops to 0.04 M, the available elemental sulfur is reduced by copper ions to form copper sulfide and stop the copper extraction [88].

Deniz et al., on the other hand, investigated the extraction rates of chalcopyrite in hydrogen peroxide and sulfuric acid in an autoclave. They determined that 2.5 M concentrations for sulfuric acid and 2.3 M concentrations for hydrogen peroxide were the most optimum parameters at a rotation speed of 630 rpm, a holding time of 24 minutes, a temperature of 78 °C, a concentration of 3.17 g chalcopyrite - 50 ml distilled water [89].

Liddicoat and Dreisinger developed two methods for copper extraction from chalcopyrite, Goethite and Hematite. The Goethite model is based on the precipitation of iron in the solution as FeOOH as a result of the reaction with air or oxygen and obtaining copper chloride ions. On the other hand, the hematite model is related to the removal of iron in the solution by converting it to Fe_2O_3 in the autoclave. For the optimization of both models, parameters such as grinding size, temperature and dwell time were examined. As a result, they obtained 95% copper extraction in the Hematite model after fine grinding of the concentrate for 4-6 hours at 95 °C (P90= 41 μm). However, it was also noted that the copper extraction from its finely ground

concentrate (P90= 37 μm) exceeded 99%. In the Gotit model, 89% copper extraction was obtained under optimum conditions in the tested atmospheric conditions [90].

4.2. NANOPARTICLES AND THEIR ELECTROCHEMICAL PROPERTIES

Saravanakumar et al used a solvothermal method to synthesize and optimize the monodispersed $CuFe_2O_4$ nanoparticles, after using different molarities of KOH, their results revealed that with 10M KOH the cyclic stability of the $CuFe_2O_4$ nanoparticles exhibits 84% retention after 100 cycles of galvanostatic charging and discharging and the pattern of the curve remains constant which indicate a very good coulomb efficiency after long cycles, and that the reduction in the size of nanoparticle increased the capacitance value. so, they conclude that with 10M KOH the $CuFe_2O_4$ nanoparticles of 20 nm size regime is a suitable electrode for pseudo captive candidate application. Their XRD and XPS test results confirm that the obtained product of their synthesis crystalizes in the tetragonal system [91].

X wu et al have synthesized the rod-like $CuFe_2O_4$ by a co-precipitation method in ethanol-water solution at room temperature, and they also studied the electrochemical performance of cufe204 as an anode material for Na-ion battery. They said that their obtained sample at 400^o c could deliver a reversible specific capacity of 281 mAh/g at a current density of 100 mA/g after 20^{th} cycle [92].

S. Polat and Dana Faris investigated and synthesized the electrochemical properties of $CuFe_2O_4$ crystals on Ni foam surface (together with g-C_3N_4, GNPs and separately), they wanted to use it as an electrode in supercapacitors, they use the hydrothermal method. According to them, these productions have been successfully realized based on their XRD, FTR and XPS analyses results in a nanosponge-like geometry. Based on their experiments, they find 989 mf/ cm^2 as the highest value of capacitance at 2mA measurement (in the presence of the three elements), their electrode stability after 1500 cycles was 70% at 16 mA, while the energy and power densities were 27,8 mWh/cm^2 and 300 mWh/cm^2 respectively. They stated that the carbon-based component increased the CS value by decreasing the charge transfer and diffusion resistances of

their electrodes.so, they concluded that the high cs value and low stability made the use of this electrode limited in low cycle application [93].

X yang et al investigated the as-synthesized product's structural and morphological properties. They used several techniques to achieve their goal, including a simple solvothermal method with subsequent calcination treatment to create porous $CuFe_2O_4$ nanospheres. They performed XRD, SEM, and TEM tests, and the XRD pattern indicates that their products were pure cubic spinel. Their SEM and TEM images show a uniform sphere-like morphology and a porous microstructure to the product. They constructed their gas sensors using the a-s prepared samples, investigated their gas sensor performance, and discovered that, when compared to pure CuO and Fe_2O_3 nanoparticles, the $CuFe_2O_4$ nanostructure exhibited superior gas sensing properties toward acetone at the operating temperature of 250^o C, including high response, outstanding selectivity and excellent response recovery property. Thus, they concluded that the $CuFe_2O_4$ nanospheres have a potential application for fabricating high performance acetone gas sensors [94].

Yan Guo et al used tween to modify $CuFe_2O_4$ ($CuFe_2O_4$-T) nanoparticles by hydrothermal method. According to them, the modification lead to a high purity of $CuFe_2O_4$-T, reduced the particle size to 10-20 nm of diameter and decrease the bandgap energy. They found that $CuFe_2O_4$-T shows improved supercapacitors behavior with a specific capacitance of 437.3F/g the scan rate of 0.004 N S^{-1} in 0.5M H_2SO_4 electrolyte, 88.6% capacitance stability retention over 2000 cycles. They claimed that tween improved greatly the performance of $CuFe_2SO_4$ nanoparticles, and their combination will have great promise for wide electrochemical application [95].

PART 5

EXPERIMENTAL PROCEDURE

5.1. MATERIALS AND METHODS

5.1.1. Materials

The chalcopyrite particles used in this thesis study were obtained from Kastamonu Hanönü region with 1-6 μm particle size as seen in Figure 5.1. It was then stored in capped plastic containers after drying at 60 °C. In the experiments, deionized water, sodium chloride (NaCl), magnesium chloride ($MgCl_2$) and urea (CH_4N_2O) were used for copper and iron extraction from chalcopyrite. Deionized water has a conductivity of 18.25 Mohm and was supplied from four resinous MARGEM water purifiers. NaCl and $MgCl_2$ were obtained from Rokkim, and urea was obtained from Aromel chemical company. After extraction, nanoparticle synthesis processes were carried out on the nickel foam surface obtained from the Nanography company. Nanoparticle synthesis was carried out in a Teflon lined stainless steel autoclave. All laboratory equipment and analysis devices used in this study were carried out at Karabuk University Materials Research and Development Center (MARGEM).

Figure 5.1. The image of chalcopyrite used in experiments.

5.1.2. Extraction of Chalcopyrite

In this part of the study, the processes of preparing solutions with different parameters for the extraction of copper (Cu) and iron (Fe) elements from chalcopyrite are explained. For this purpose, firstly, a 250 ml beaker was taken, and 50 ml of deionized water was added into it, and the beaker containing this mixture was placed on the heater and waited by magnetic stirring until its temperature reached 60 °C. When the temperature reached 60 °C, 6-gram chalcopyrite was added by weighing into the beaker. Stirring was continued for one hour at the same temperature. After this process, the mixture was taken over the heater and filtered on Watman filter paper with the help of a funnel. The filtrate was centrifuged at 3000 rpm for 15 minutes to avoid residual particles. Thus, the extraction process is completed. On the other hand, NaCl and $MgCl_2$ were also used separately as a secondary reactant to examine the effect on the concentration of Cu and Fe elements in the extraction solution. These reactants were added to the solution together with the chalcopyrite in the amounts in table 1. Then, the amounts of NaCl and $MgCl_2$ were determined, where the highest values were obtained in terms of Cu and Fe concentrations. After that, urea was added in the amounts in Table 1 together with the highest concentration of $MgCl_2$, and thus the effect of urea was also examined. All of these operations were carried out in the setups given in Figure 5.2.

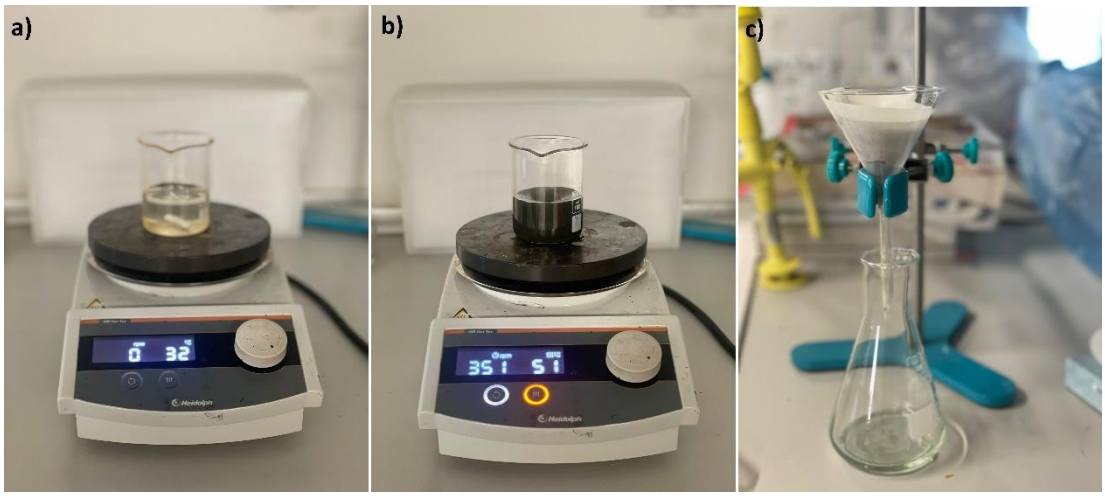

Figure 5.2. a-b) Extraction preparations and b) after filtration.

5.1.3. Cu and Fe Concentration Measurements

The copper (Cu) and iron (Fe) concentrations of the solutions (stock solutions) obtained after extraction were determined by THERMO SCIENTIFIC ICE 3400 atomic absorption spectrometers (AAS). This process was first started by dilution into stock solutions. The purpose of this dilution is because the Cu and Fe concentrations in the stock solutions are above the AAS measurement limit. For this process, firstly, 500 microliters of stock solutions were taken and mixed with 50 ml of deionized water and 5 M measurement solutions were prepared. These samples were called dilute solutions. On the other hand, for the measurement, other solutions of 1 ppm, 3 ppm and 5 ppm were prepared separately from 1000 ppm Cu and Fe standard solutions with the same dilution process, and these were called calibration solutions. Measurements were made using the flame measuring part of the device and Cu and Fe cathode tubes. First, the Cu tube was activated, and it was waited for about 15 minutes for it to become stable. Then, a method was created, with the first three measurements consisting of calibration solutions and the following from dilute measurement samples. Measurements were started with this method and firstly, the concentrations of 1 ppm, 3 ppm and 5 ppm standard solutions were measured. According to the results in the flame measurement standard of the Cu element in the software, it was stated that it should give 0.4 absorbance at 1 ppm concentration and the measurement results of the standard solutions were obtained in this direction. Then, the method was terminated by measuring the dilute measurement samples. The same procedure was carried out for Fe. With the results obtained here, the Cu and Fe concentrations of the stock solutions were calculated in ppm units with a simple ratio. The same measurement procedure was applied to all stock solutions after extraction. The solutions prepared by the AAS device used for this purpose are given in Figure 5.3 and Figure 5.4.

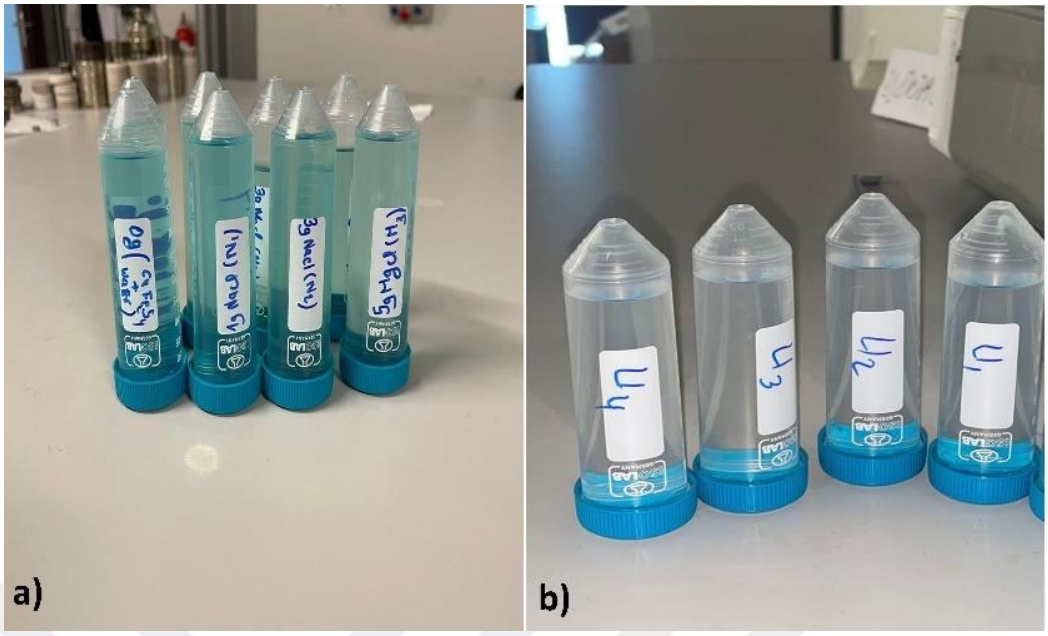

Figure 5.3. a) Post-extraction solutions and b) diluted solutions for AAS measurement.

Figure 5.4. Atomic absorption spectroscopy (AAS).

5.1.4. Nanoparticle Synthesis

The use of Cu and Fe in solutions after the extraction of minerals rich in Cu and Fe such as chalcopyrite is also very important for the purpose of such studies. For this purpose, although the aforementioned elements are commonly tried to be obtained in metallic form, it is highly needed in some areas to obtain them as metal oxides. Especially in supercapacitors, nanosized metal oxide synthesis on a metal collector substrate surface is very important in terms of energy storage performance. For this reason, in this part of the study, it is aimed to synthesize Cu-Fe-based metal oxide nanoparticles from the solution, which has the highest concentration of Cu and Fe extraction from chalcopyrite, based on the information in the literature. It is aimed to use the nanoparticles supercapacitors to be synthesized at this stage to store electrical energy at the anode electrode. For this reason, it must be synthesized on a conductive substrate. One of the most common conductive substrate materials used in supercapacitors is nickel foam, which has a very large surface area. In this study, it is aimed to synthesize metal oxide nanoparticles, which are expected to consist of Cu and Fe, on nickel foam. Hydrothermal method is one of the most suitable methods that can provide nanoparticle synthesis in liquid environment and on a substrate . Before starting the productions with this method, the solution with the highest concentration obtained in the previous step was determined first. Then, 10 ml of this solution was taken and added to a Teflon lined stainless steel autoclave with a capacity of 40 ml. At the same time, 2 pieces of nickel foam cut in 1x3 dimensions were added to this autoclave. Then, first the lid of the Teflon liner and then the lid of the stainless-steel autoclave was tightly closed. The same processes were applied in another two autoclaves, and a total of three autoclaves were prepared for the productions. Afterwards, the autoclaves were placed in the oven and heated up to 150 °C at a heating rate of 10 °C and waited at that temperature for 6 hours. After this process, the autoclaves were removed from the oven and allowed to cool down to room temperature. Then, the covers were opened, and the nickel foams were taken out and washed with deionized water to remove the residues on it. Then, it was placed in an oven on a watch glass and dried at 60 °C for one day and dehumidified. In addition, since the solutions in the autoclave also contain synthesized product particles and can be used in the characterization processes, they were taken into glass tubes and

centrifuged at 3000 rpm for 15 minutes. Then, the remaining liquid was poured out and the particles remaining as precipitate were dried in the oven for one day. Thus, the production processes on nickel foam were carried out. The representation of the experimental setup and equipment used during production is given in Figure 5.5 and Figure 5.6.

Figure 5.5. Hydrothermal sample preparations with extracted solution.

Figure 5.6. Macro view before and after CFO coating with hydrothermal method.

5.1.5. Material Characterization

For the characterization of the products obtained after the metal oxide synthesis process on the nickel foam surface with the hydrothermal method, firstly, crystallographic analysis was performed with the Rigaku Ultima IV X-ray diffraction (XRD) device. In these analyzes, Cu-based Ka radiation (λ = 0.1546 nm) with a fixed monochromator at 40 kV and 40 mA with a 2θ value in the range of 10-80° was used. Then, for the chemical bond analysis of these products, analyzes were made between 400-4000 cm-1 wave number with 2 cm-1 resolution in transmission mode with Bruker Alpha brand Fourier transform infrared spectroscopy (FTIR). In addition, the microstructure and morphological images of these components were examined with Carl Zeiss ULTRA PLUS Scanning Electron Microscope (SEM). The representations of the devices used for this purpose are given in Figure 5.7, Figure 5.8 and Figure 5.9, respectively.

Figure 5.7. X-ray diffraction instrument (XRD).

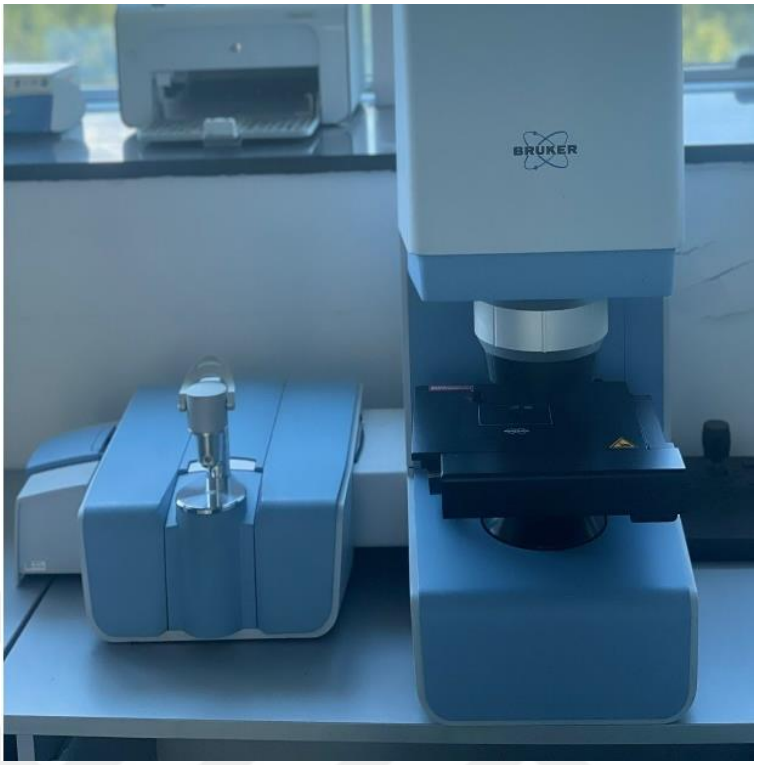

Figure 5.8. Fourier transform infrared spectroscopy (FTIR).

Figure 5.9. Scanning electron microscope (SEM).

5.1.6. Electrochemical Measurements

Electrochemical performances of metal oxides synthesized directly on nickel foam surface by hydrothermal method from extraction solution were investigated with Parstat 4000 brand potentiometer device at room temperature. A three-electrode test unit was used in these analyses. Graphite was used as counter electrode, Ag/AgCl as reference electrode and metal oxide doped nickel foam as working electrode as seen in Figure 5.10. Measurements were carried out in 6 M KOH solution. This solution was prepared with 18.25 Mohm resistive deionized water. Before starting the measurements, a load of about 10 MPa was applied to the nickel foam, making it flatter. Next, the KOH solution was placed in a beaker and the electrodes were immersed in it. The working electrode, nickel foam, was adjusted to be immersed in this solution to be approximately 1 cm^2. After this process, galvanostatic charge-discharge measurements were carried out in the range of 1-6 mA using the Versa studio software program. From these measurements, the discharge times at each current density were determined. Then, specific areal capacitance (Ca) values were calculated according to the formula in Equation 5.1 [96].

$$C_s = \frac{I \times \Delta t}{\Delta V \times S} \tag{5.1}$$

In this formula, the Ca value is the area capacitance (mF), I is the discharge current constant (mA), (Δt) is the discharge time (sec), ΔV is the potential window (V), and (S) is the surface area of the working electrode in cm^2. In addition, the energy (E) and power (P) densities of the electrode were calculated according to Equations 5.2 and Equation 5.3 according to the data obtained from here.

$$E = \frac{C_s \times V^2}{7.2} \tag{5.2}$$

$$P = \frac{3600 \times E}{\Delta t} \tag{5.3}$$

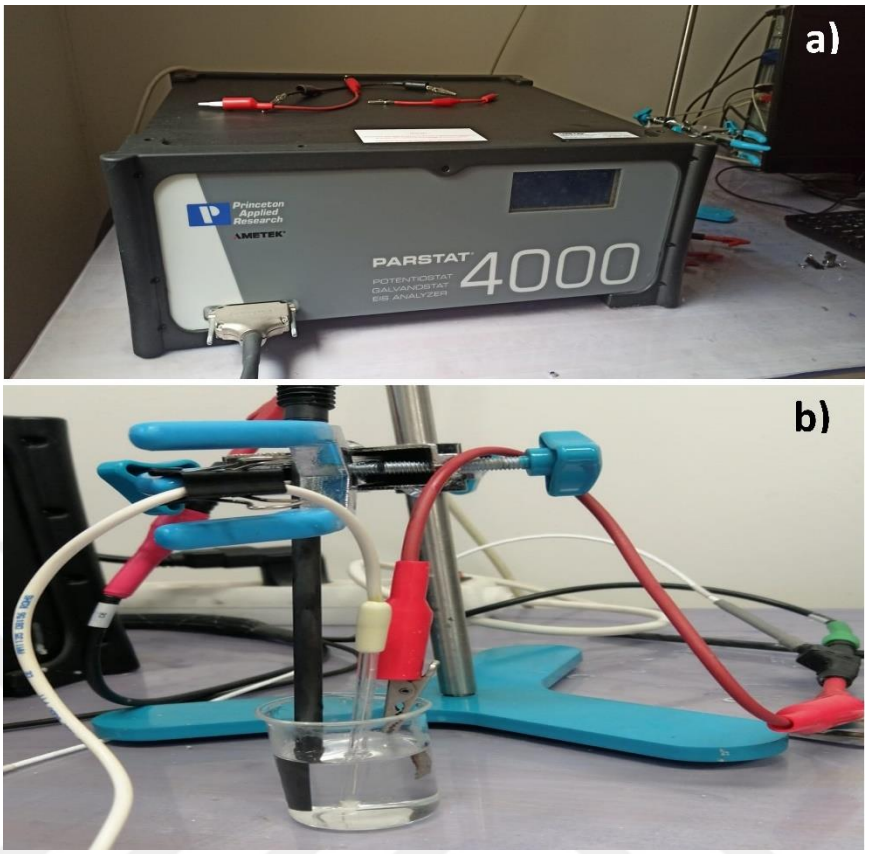

Figure 5.10. Electrochemical instruments a) Parstat 4000 , b) three-electrode cell.

PART 6

RESULTS AND DISCUSSION

6.1. EXPERIMENTAL RESULTS AND DISCUSSIONS

6.1.1 Elemental Examination of Leaching Solution with AAS

The results of Cu and Fe concentrations in the extraction solutions measured by AAS are examined in this section. The obtained results are given in detail in the graphs in Figure 6.1. The samples referred to as reference in these results belong to the extraction solution made only with deionized water without using any reactants. According to the results obtained, the Cu and Fe concentrations of the reference sample were determined as 225 mg/L and 203 mg/L, respectively. In subsequent experiments, when 1-gram NaCl was added to the extraction solution as reactant (N1), Cu and Fe concentrations were measured as 295 mg/L and 199 mg/L. According to this result, it was understood that with the addition of 1 gram of NaCl, the extraction of Cu increased by %31, and Fe decreased by 2%, respectively. Then, solutions containing 3-gram (N3), 5-gram (N5), 7-gram (N7) and 9-gram (N9) NaCl were prepared to determine the changes in the extraction rate depending on the amount of reactant. Cu concentrations in these solutions were measured as 306 mg/L, 333 mg/L, 380 mg/L and 400 mg/L, respectively, while Fe concentrations were found to be 205 mg/L, 221 mg/L, 242 mg/L and 261 mg/L. Based on these results, it can be said that the concentration of Cu and Fe increased between 76% and 28%, respectively. The relationship of these increase amounts with the increase in the amount of NaCl was also given in the graph in Figure 6.1a and b. The slopes of the lines in this graph were also calculated as 0.86 for Cu and 0.34 for Fe. Thus, if it is desired to prepare an extraction solution at higher or lower concentrations, it will be possible to determine how much NaCl should be used and how much Cu and Fe extraction can be achieved by using the slopes of these lines.

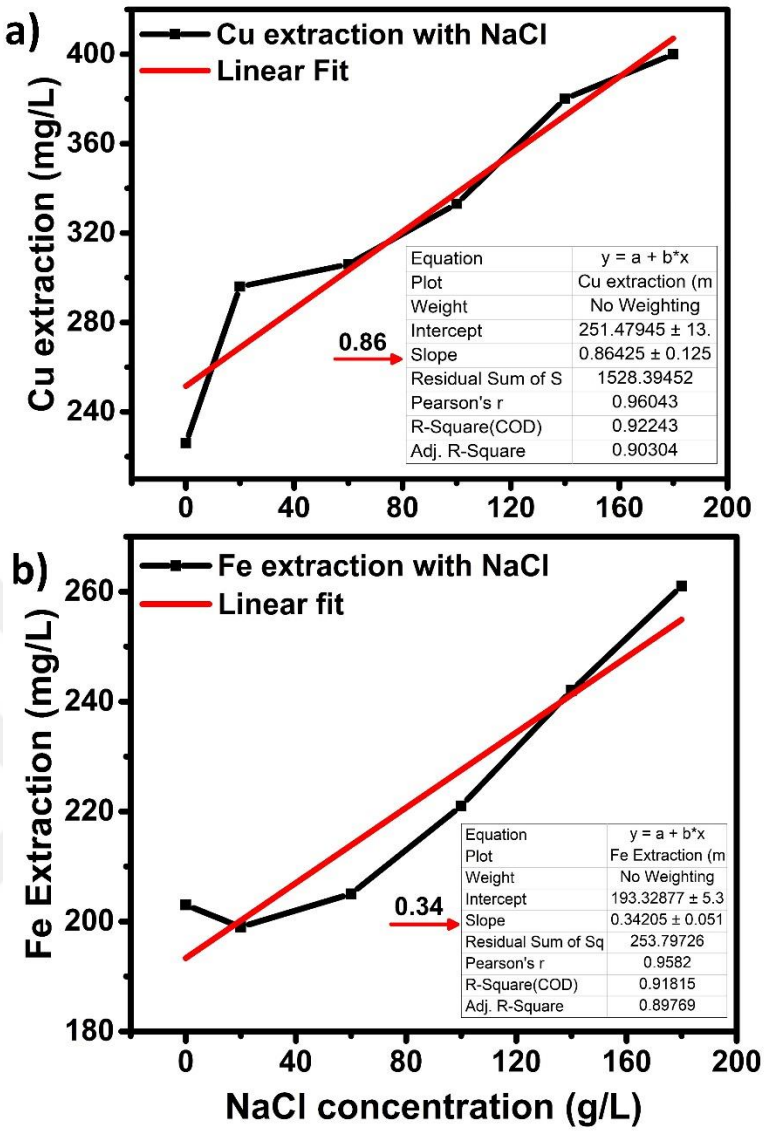

Figure 6.1. Concentrations of a) Cu and b) Fe with the addition of NaCl to the extraction solutions.

The effect of $MgCl_2$, a metal chloride salt of group 2A, as a similar but different component was also investigated. Similarly, solutions containing 1-3-5-7-9-gram $MgCl_2$ were prepared to determine the changes in the extraction rate depending on the amount of $MgCl_2$ under the same conditions, and these solutions were named M1, M3, M5, M7, and M9, respectively. The results were given in Figure 6.2. According to these results, Cu concentrations for M1, M3, M5, M7, and M9 were determined as 318 mg/L, 329 mg/L, 336 mg/L, 345 mg/L and 322 mg/L, respectively, while Fe concentration was 220 mg/L, 223 mg/L, 299 mg/L, 311 mg/L and 286 mg/L. The concentration increases for both elements increased up to the M7 sample, and then

decreased. The amount of increase for Cu and Fe was observed as 52% and 53%, respectively. In this case, it can be said that $MgCl_2$ decreases the Cu extraction but increases the Fe extraction compared to NaCl. It was also observed that unlike NaCl, after a certain level (7 grams), it reduced the extraction of Cu and Fe by approximately 6% and 8%, respectively.

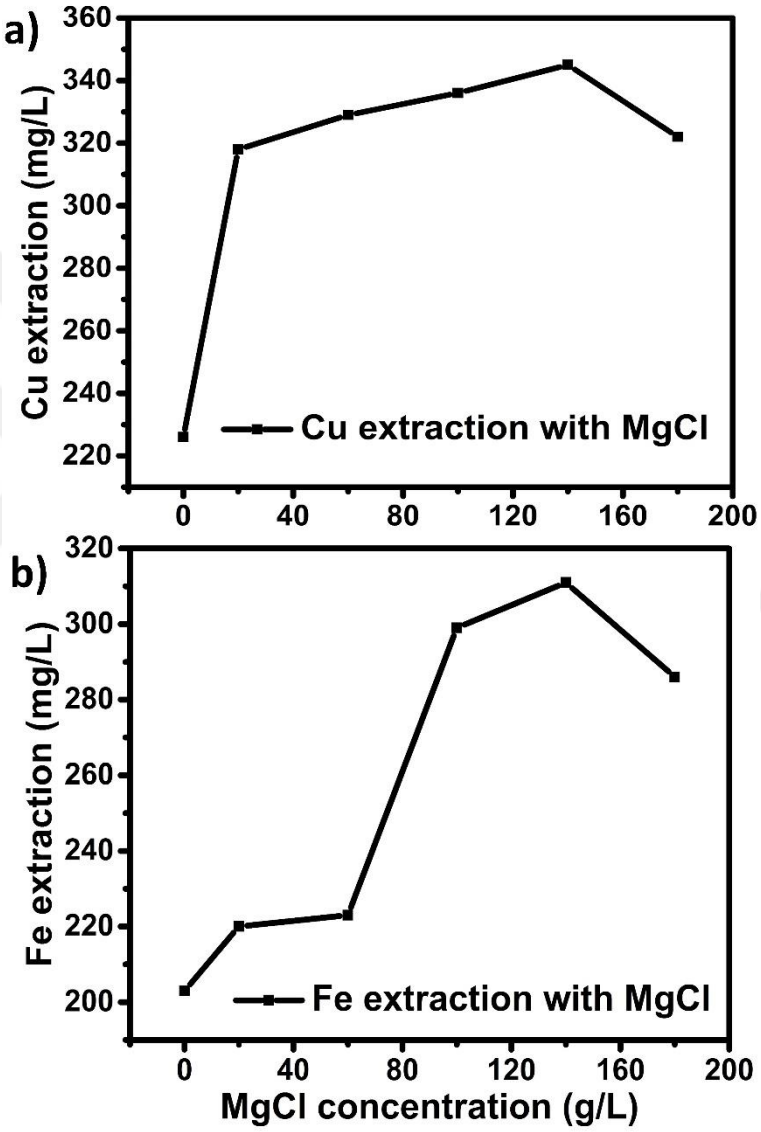

Figure 6.2. Concentrations of a) Cu and b) Fe with the addition of $MgCl_2$ to the extraction solutions.

Another parameter used in experimental studies is on the combination of two reactants. For this reason, considering that the Cu and Fe concentration of $MgCl_2$ could be increased, it was decided to use $MgCl_2$ together with urea. As a secondary reactant,

urea (CH_4N_2O), a component that can absorb sulfur in chalcopyrite, was chosen and the amount to be used was determined as 1-grams, 3-grams, 5-grams, 7-grams and 9-grams. On the other hand, the amount of $MgCl_2$ to be used with urea was chosen as M7 (7 grams), which represents the highest Cu and Fe concentration, and these samples were named M7U1, M7U2 and M7U3. The obtained results from these experiments were given in Figure 6.3. According to these results, Cu concentrations of M7U1, M7U3, M7U5, M7U7 and M7U9 samples were determined as 373 mg/L, 354 mg/L, 324 mg/L, 314 mg/L and 303 mg/L, respectively, while Fe concentrations were determined as 258 mg/L, 239 mg/L, 208 mg/L, 203 mg/L and 202 mg/L. Compared to the M7 sample, these results increased by 8% for Cu and after that this value decreased up to 12% by M7U9. At the same time Fe concentration directly decreased with urea up to 35%. As a result, it was observed that $MgCl_2$ increased the Cu concentration slightly compared to NaCl and even decreased it after a certain rate, while it also increased the Fe concentration significantly. On the other hand, it was observed that the urea additive started to decrease these concentrations directly after 1 gram, and the Fe concentration in these solutions was lower compared to Cu.

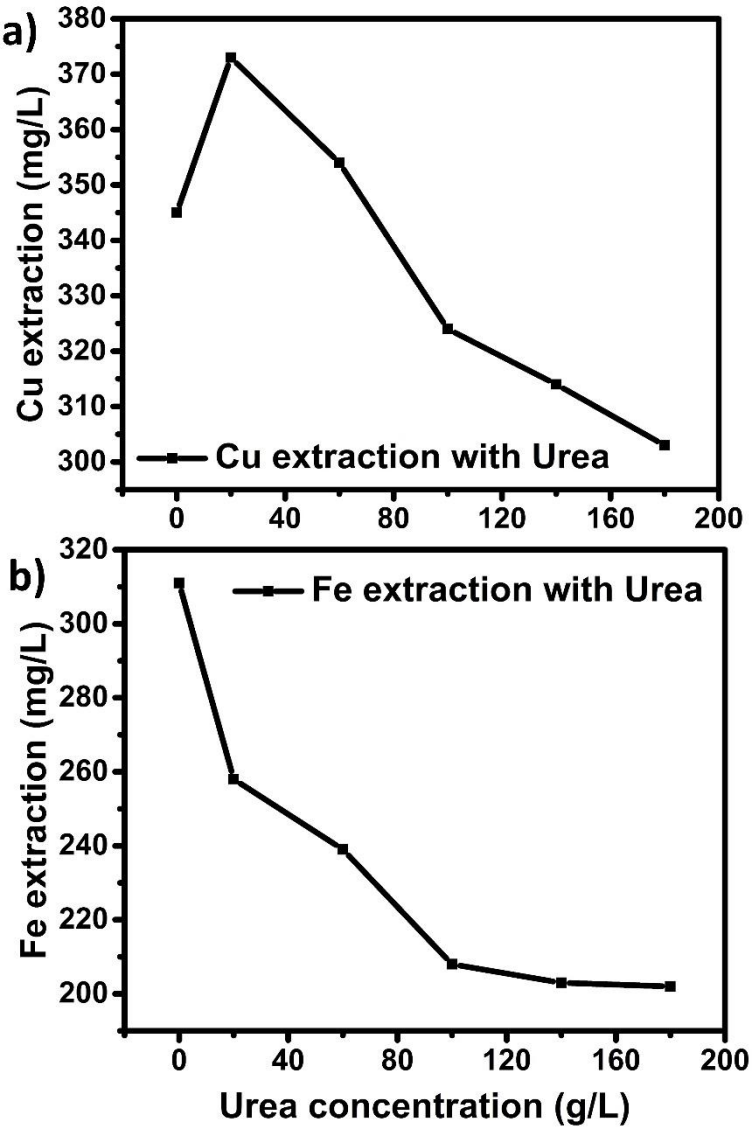

Figure 6.3. Concentrations of a) Cu and b) Fe with the addition of $MgCl_2$ + Urea to the extraction solutions.

6.1.2 XRD and FTIR Analysis of Cu-Fe Metal Oxide Nanoparticles

The crystal structure and chemical bond analysis of metal oxide nanoparticle crystals synthesized directly on the nickel foam surface were performed by XRD analysis. The result of this analysis was given in Figure 6.4. According to the XRD graph, sharp peaks were observed at 2θ value at 35°, 39°, 43°, 55°, 60° and 64°, which probably belong to the (311), (222), (400), (511), (440) and (300) planes of the spinel-structured $CuFe_2O_4$ compound [97,98]. At the same time, other peaks were also observed at 11°, 17°, 22°, 26° and 32°, which probably belong to the (110), (211), (112), (301), and

(312) planes of urea and at 16° and 17°, 19° the (200) and (211) planes of thiourea, respectively [99]. On the other hand, FTIR result was given in Figure 6.5. According to the result, two sharp peaks were observed at wave numbers 456 cm^{-1} and 598 cm^{-1}, representing Cu-O and Fe-O bonds, respectively [100]. Apart from these, extra peaks were also observed at 1082 cm^{-1}, 1409 cm^{-1}, 1558 cm^{-1}, 1627 cm^{-1} and 598 cm^{-1}, indicating the presence of carbon-like and NH_2 compounds. Similarly, the flat peak observed at 3095 cm^{-1} represents O-H bonding, probably due to moisture in the structure [99].

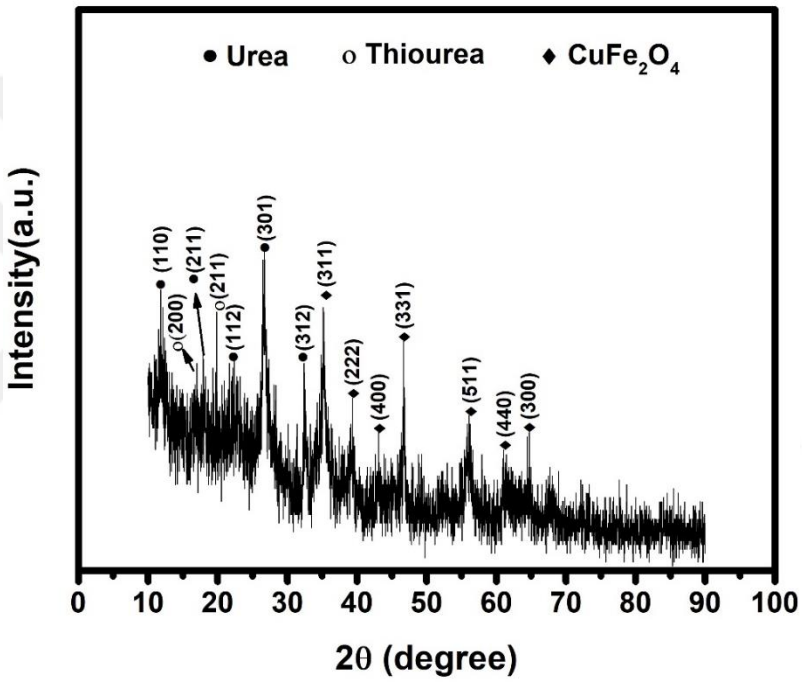

Figure 6.4. XRD result of synthesized CFO nanoparticles.

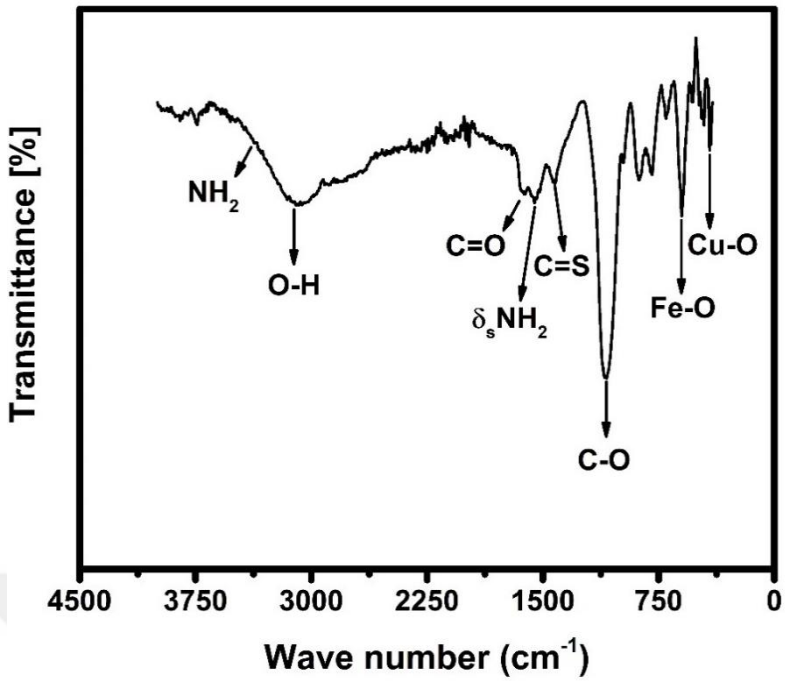

Figure 6.5. FTIR result of synthesized CFO nanoparticles.

6.1.3 Surface Microstructure Analysis of Nanoparticles by SEM

The microstructure of Cu-Fe-based metal oxide nanoparticles synthesized on the nickel foam surface was examined by SEM, and the results are given in the visuals in Figure 6.4. A general view of untreated and treated nickel foam is given in the image in Figure 6.4a and Figure 6.4b, respectively. As can be seen from these images, a formation has occurred on the nickel foam surface. In the higher magnification images given in Figure 6.4c and Figure 6.4d, it can be said that these formations are plate-shaped and rose-patterned. While the wall dimensions of these plates were measured at around 100 nm, the wall thickness was determined as 44 nm as seen in Figure 6.4c. It can be said that these very thin-walled, and nano-sized structures mainly consist of $CuFe_2O_4$ crystal structures according to XRD and FTIR analysis. Literature data also confirm these results.

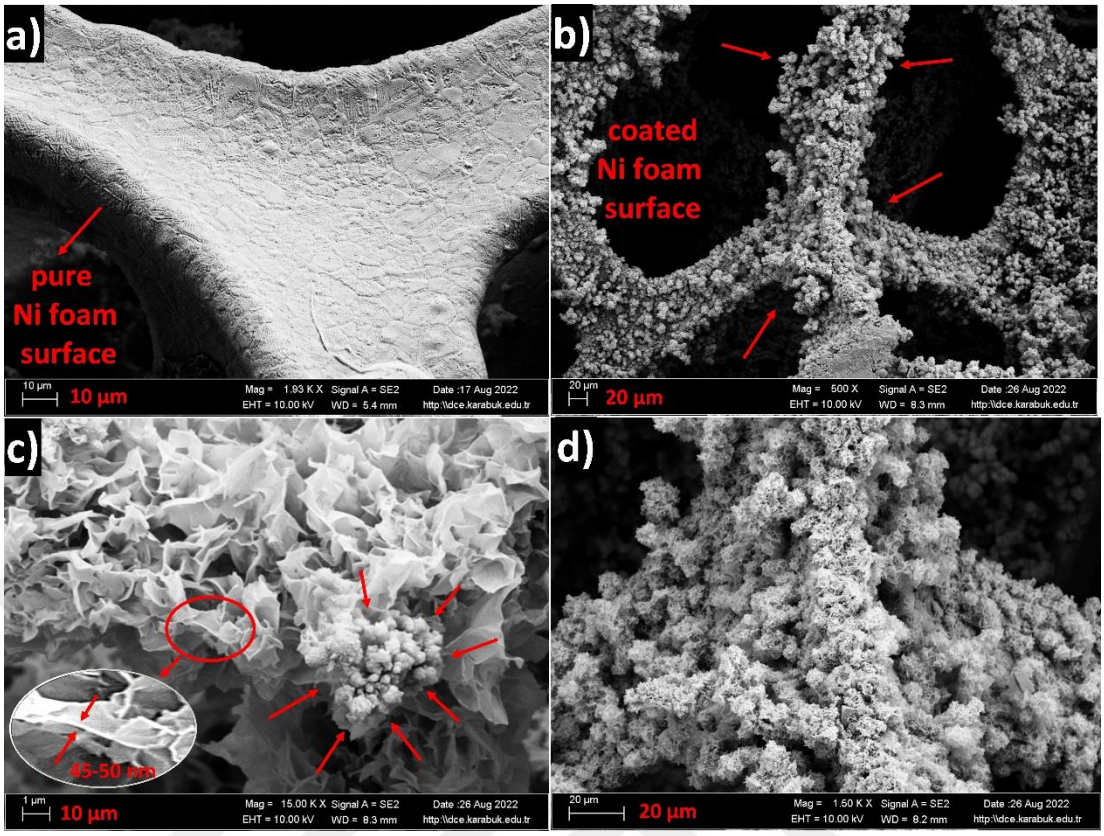

Figure 6.6. SEM images of a) pure Ni foam, and b-c-d) high magnified CFO coated Ni foam.

6.1.4 Electrochemical Measurement Results

The synthesis of Cu-Fe metal oxide nanoparticles directly on the nickel foam surface by hydrothermal method from the extraction solution was confirmed by XRD, FTIR and SEM analyses. The samples obtained here were produced to be used as anode electrodes for energy storage in supercapacitors. In this title, the electrochemical performances of nickel foam electrodes synthesized with metal oxide nanoparticles on the surface were investigated for this purpose. For this purpose, galvanostatic charge-discharge measurements were carried out at current densities of 1 mA, 2 mA, 3 mA, 4 mA, 5 mA, 8 mA, and 10 mA, and the results were given in Figure 6.7. The discharge times obtained at these current densities were measured as 251 sec, 163 sec, 107 sec, 82 sec, 46 sec, and 35 sec, respectively. In addition, depending on this electrode's discharge times, the specific areal capacitance values (Ca) at each current value were calculated as 725 mF, 702 mF, 605 mF, 575 mF, 525 mF, and 485 mF, as seen in Figure 6.8. According to these results, the highest performance for energy storage was

obtained at 2 mA current value. On the other hand, this electrode's energy and power densities were also calculated and given in Figure 6.9. According to the results obtained here, the energy densities in each current density from 2 mA up to 10 mA were determined as 12.5 mWh/cm^2, 11.9 mWh/cm^2, 10.3 mWh/cm^2, 9.7 mWh/cm^2, 8.9 mWh/cm^2, and 8.2 mWh/cm^2, respectively. At the same time, the power density of the electrode from 2 mA up to 10 mA were calculated as 12.5175 mWh/cm^2, 262 mWh/cm^2, 350 mWh/cm^2, 437 mWh/cm^2, 700 mWh/cm^2, and 875 mWh/cm^2 as seen in Figure 6.9. As in specific capacitance, the highest energy and power density values were obtained at 2 mA current.

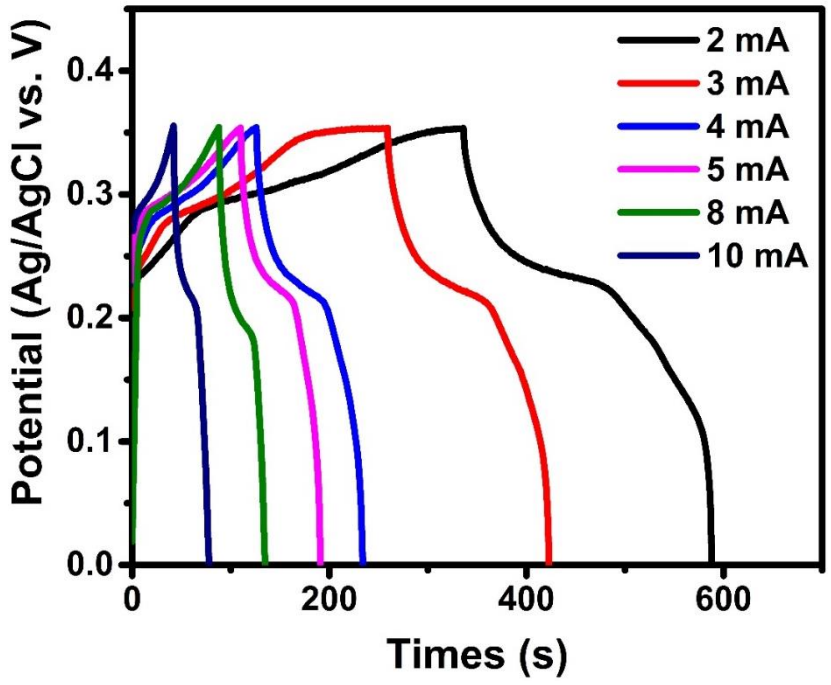

Figure 6.7. Galvanostatic charge – discharge measurements.

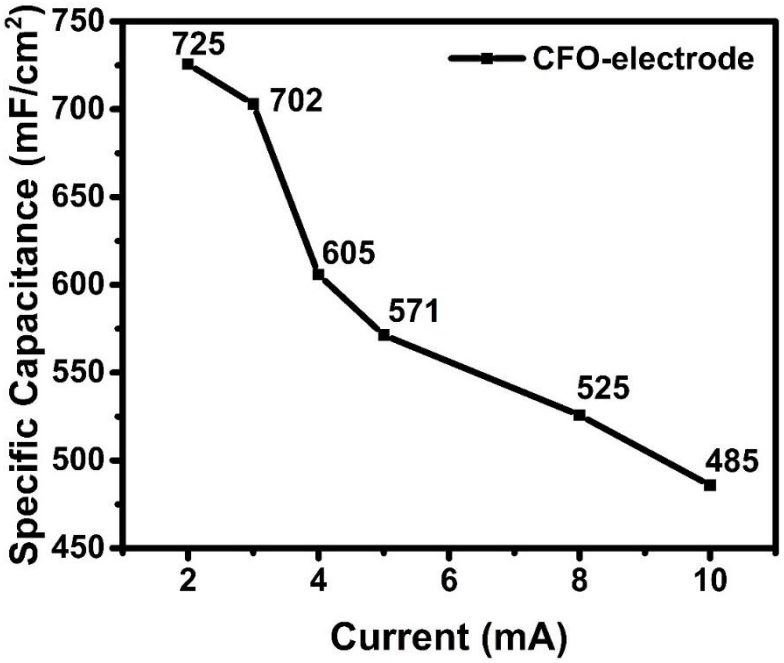

Figure 6.8. Calculated specific capacitance measurements.

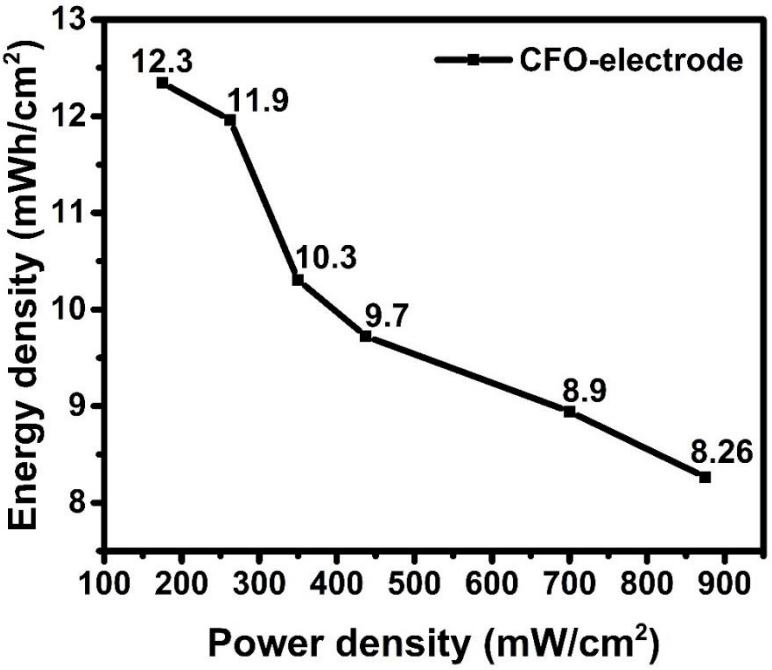

Figure 6.9. Calculated energy and power density.

6.2. DISCUSSIONS

The first issue discussed in this study was the effect of NaCl, $MgCl_2$ and urea reactants on the extraction of Cu and Fe from chalcopyrite. These studies showed that NaCl increased the Cu and Fe concentration by 76% to 26% compared to $MgCl_2$. In this context, Ruiyang Zhang et al. found the highest copper concentration to be approximately 250 mg/L in their investigation for NaCl, KCl, $MgCl_2$ and $CaCl_2$ salts [101]. In this study, a maximum of 400 mg/L was reached with NaCl. For this reason, it can be said that a significant advantage is provided. In addition, the lower Cu and Fe concentrations with $MgCl_2$ addition compared to NaCl are in line with Ruiyang Zhang et al. However, the quantitative ratios examined in this study revealed that $MgCl_2$ decreases the Cu and Fe concentration after a certain point, which is an important contribution to the literature. In addition to these, it can be said that the addition of urea together with $MgCl_2$ has a negative effect in terms of Cu concentration, while it has a positive effect because it reduces the ratio of Fe in the solution.

On the other hand, the charging mechanism of a supercapacitor electrode is realized by two different mechanisms: electrochemical double-layer capacitance (EDLC) and pseudocapacitive (PC). Among them, EDLC is related to the absorption of ions in the environment on the surface [91,102–104]. Therefore, it can be said that the large surface area of the electrode increases its performance. Pc, on the other hand, is associated with the reduction/oxidation reactions of ions while adhering to the surface. In this context, the Cu and Fe-based electrode produced in this study is very advantageous in terms of Pc properties because this property of metal oxides has been expressed in the literature. In addition, it is thought that the synthesis of copper ferrite by hydrothermal method without using any binder on the surface covers a large surface area and improves the performance by contributing to the charging mechanism in terms of EDLC feature. On the other hand, in the studies done so far, Ham et al. He stated that $CuFe_2O_4$ (CFO) is one of the most important factors affecting the redox reaction and specific capacitance of its active ends [105]. In this context, they made a CFO coating with the spray pyrolysis method in their study and concluded that the porosity significantly affects the active tips. Due to the low porosity of their coating, they achieved a very low specific capacitance (Ca) of 5.7 F/g at a current density of

0.3 μm/cm2. On the other hand, to increase the performance by increasing ionic diffusion to these active tips, Zhao et al. He synthesized CFO in nanotube form and determined the Cs value as 28 F/g at a current density of 0.5 A/g [106]. However, these values indicated that they left the CFO far behind their counterparts. For this reason, some experiments were carried out with syntheses in different geometric forms and with different components, and the results of the leading ones are given in Table 3 in detail. It has been understood that the Ca values of CFOs produced in spherical geometry are around 189 to 345 F/g. However, when two-dimensional carbon-like materials such as graphene [107–109] are added, it is observed that the Ca performance reaches 576 F/g to 989 mF/cm^2. In these studies, it was stated that graphene's two-dimensional and conductive nature caused CFO to interact with more ions by expanding both its conductivity and surface area, and an increase in Ca value. However, as in this study, the production of CFO at nanoscale and the presence of small amounts of urea and thiourea additives increased the Ca performance up to 725 mF/cm^2. These results show that the produced electrode is very promising, but the multiple cycle results should also be examined.

Table 6.1. Some results in terms of electrochemical performance of $CuFe_2O_4$ used as an electrode in the literature.

Electrode materials	**Electrolyte solution**	**Specific Capacitance**	**Capacitance retention (%)**	**Ref.**
CFO	6M KOH	725 F/cm^2 at 2 mA/cm^2	-	This study
CFO-4	6M KOH	989 F/cm^2 at 1.3 mA/cm^2	73.3% after 1500 cycles	[93]
$CuFe_2O_4$-GN	3M KOH	576.6 F/g at 1 A/g	85% after 1000 cycles	[110]
$CuFe_2O_4$/tween-80	0.5M H_2SO_4	437.3 F/g at 4 mV/s	88.6% after 2000cycles	[111]
$CuFe_2O_4$ nanospheres	1 M KOH	345 F/g at 0.6 A/g	88% after 600 cycles	[112]
Nano spherical $CuFe_2O_4$	2 M KOH	189.2 F/g at 0.5 A/g	84% after 1000 cycles	[91]

PART 7

SUMMARY

This thesis work consists of two parts. In the first part, the extraction of chalcopyrite, which is used as an important source of copper, is discussed. For this purpose, the studies on copper and iron extraction from chalcopyrite were examined, and the problems were determined. At the beginning of these, it was stated that the use of expensive reactants and the oxidation of the sulphur in the chalcopyrite during the extraction and forming a passivation layer on the surface. In order to solve these problems, chlorine sources such as NaCl and $MgCl_2$, which are cheaper and especially advantageous in Cu extraction, have been used. In addition, urea compound, which can be converted into thiourea by absorbing sulphur with these salts, was also used. Extractions were achieved by the hydrometallurgical method by changing the amount of each reactant, and the conditions were optimized by determining the maximum points of Cu and Fe concentrations. According to these results, Cu and Fe concentrations increased by 76% and 28%, respectively, with the addition of 1 g to 9 g of NaCl to the solution, while they increased by 52% and 53% with the addition of $MgCl_2$. In addition, when urea was added to $MgCl_2$, the Cu concentration initially increased by around 8%, then decreased to 12%, while the Fe concentration directly decreased to 35%.

On the other hand, the presence of only copper and iron in the extraction solution has also been expressed as a pollution problem. The problem of the presence of iron in the solutions aims to be turned into an advantage by synthesizing the copper ferrite compound of copper and iron in this thesis, because copper ferrite can be used as a cheap and easily synthesized anode electrode material in supercapacitors as given in literature. For this reason, hydrothermal method was used for the synthesizing of copper ferrite nanoparticles directly on the nickel foam surface from the extraction solution with the highest Cu and Fe concentrations. After that, the obtained samples

were characterized by FTIR, XRD, and SEM. While the chemical and crystal structures of urea, thiourea, and copper ferrite compounds were observed in FTIR and XRD results, nano-sized copper ferrite formations in the form of plates with a wall thickness of approximately 50 nm were observed in the SEM analysis. After these processes, the electrochemical performances of the produced electrode were investigated. As a result, it was calculated the specific capacitance of produced electrode as 725 mF/cm^2, an energy density of 12.5 mWh/cm^2, and power density of 880 mW/cm^2. When these results are compared with the literature, it is concluded that it is a very high-capacity electrode material obtained only with copper ferrite without adding extra carbon-like additives. For this reason, it is concluded that it is a promising electrode material if its dimensional optimization is provided, and its electrochemical performance is examined in detail with multiple cycles.

REFERENCES

1. Wang, P., Li, N., Li, J., and Chen, W.-Q., "Metal-energy nexus in the global energy transition calls for cooperative actions", The Material Basis of Energy Transitions, ***Elsevier***, 27–47 (2020).

2. "Bilim Teknik", **https://bilimteknik.tubitak.gov.tr/makale/mineral-ve-metallerin-insan-hayatindaki-onemi** (2022).

3. "Mining & Mineral Usage Statistics", **https://chrisr250.sg-host.com/mining-mineral-statistics/** (2022).

4. "Minerals In Your Life", **https://chrisr250.sg-host.com/mining-minerals-information/minerals-in-your-life/** (2022).

5. Frenzel, M., Tolosana-Delgado, R., and Gutzmer, J., "Assessing the supply potential of high-tech metals – A general method", ***Resources Policy***, 46: 45–58 (2015).

6. YATMAZ, P. I. and KESİM, B., "SOY OLMAYAN METALLERE BAĞLANAN İKİ ADEZİV SİSTEMİN KESME KUVVETLERİNE KARŞI DİRENÇLERİNİN İNCELENMESİ", .

7. Yılmaz, M. G., "Solvent Ekstraksiyon Yöntemi İle Atık Çözeltilerden Soy Metallerin Geri Kazanımı", PhD Thesis, ***Fen Bilimleri Enstitüsü***, (2005).

8. Şenol, Ç. and Kervan, N., "RbX (X= Sb, Te) bileşiklerinin manyetik özelliklerinin yoğunluk fonksiyonel teorisi ile incelenmesi", Master's Thesis, ***Nevşehir Hacı Bektaş Veli Üniversitesi***, (2013).

9. Strezov, V., Zhou, X., and Evans, T. J., "Life cycle impact assessment of metal production industries in Australia", ***Scientific Reports***, 11 (1): 1–9 (2021).

10. "Bakır", **https://bilimgenc.tubitak.gov.tr/periyodik-tablo/bakir** (2022).

11. "MTA Genel Müdürlüğü", **https://www.mta.gov.tr/v3.0/metalik-madenler/bakir** (2022).

12. "It's Elemental - The Element Iron", **https://education.jlab.org/itselemental/ele026.html** (2022).

13. Vermylen, C., "What is new in iron overload?", ***European Journal Of Pediatrics***, 167 (4): 377–381 (2008).

14. Sun, W., Wang, Q., Zhou, Y., and Wu, J., "Material and energy flows of the iron and steel industry: Status quo, challenges and perspectives", ***Applied Energy***, 268: 114946 (2020).

15. Bahar, N., "Copper Recovery from Roasted Chalcopyrite Concentrate by Using Hydrochloric Acid or Water Leaching Method", ***International Journal Of Pure And Applied Sciences***, 1 (1): 1–8 (2015).

16. Polyakov, E. G. and Sibilev, A. S., "Recycling rare-earth-metal wastes by pyrometallurgical methods", ***Metallurgist***, 59 (5): 368–373 (2015).

17. HABASHİ, F., "Çeviren: Mehmet CANBAZOĞLU (***)", .

18. Balagurov, A. M., Bobrikov, I. A., Maschenko, M. S., Sangaa, D., and Simkin, V. G., "Structural phase transition in CuFe2O4 spinel", ***Crystallography Reports***, 58 (5): 710–717 (2013).

19. Moskalyk, R. R. and Alfantazi, A. M., "Review of copper pyrometallurgical practice: today and tomorrow", ***Minerals Engineering***, 16 (10): 893–919 (2003).

20. Laputka, M. and Xie, W., "A Review of Recent Advances in Pyrometallurgical Process Measurement and Modeling, and Their Applications to Process Improvement", ***Mining, Metallurgy & Exploration***, 38 (2): 1135–1165 (2021).

21. Anindya, A., Swinbourne, D. R., Reuter, M. A., and Matusewicz, R. W., "Distribution of elements between copper and FeOx–CaO–SiO2 slags during pyrometallurgical processing of WEEE", ***Mineral Processing And Extractive Metallurgy***, 122 (3): 165–173 (2013).

22. Agrawal, A., Kumar, V., Pandey, B. D., and Sahu, K. K., "A comprehensive review on the hydro metallurgical process for the production of nickel and copper powders by hydrogen reduction", ***Materials Research Bulletin***, 41 (4): 879–892 (2006).

23. Radmehr, V., Koleini, S. M. J., Khalesi, M. R., and Tavakoli Mohammadi, M. R., "Ammonia Leaching: A New Approach of Copper Industry in Hydrometallurgical Processes", ***Journal Of The Institution Of Engineers (India): Series D***, 94 (2): 95–104 (2013).

24. Sole, K. C., Mooiman, M. B., and Hardwick, E., "Ion Exchange in Hydrometallurgical Processing: An Overview and Selected Applications", ***Separation & Purification Reviews***, 47 (2): 159–178 (2018).

25. Gunarathne, V., Rajapaksha, A. U., Vithanage, M., Alessi, D. S., Selvasembian, R., Naushad, Mu., You, S., Oleszczuk, P., and Ok, Y. S., "Hydrometallurgical processes for heavy metals recovery from industrial sludges", ***Critical Reviews In Environmental Science And Technology***, 52 (6): 1022–1062 (2022).

26. Yao, Y., Zhu, M., Zhao, Z., Tong, B., Fan, Y., and Hua, Z., "Hydrometallurgical Processes for Recycling Spent Lithium-Ion Batteries: A Critical Review", ***ACS Sustainable Chemistry & Engineering***, 6 (11): 13611–13627 (2018).

27. Velásquez, L. and de Lourdes, L., "The kinetics of dissolution of chalcopyrite in chloride media", ***Murdoch University: Perth, Australia***, 291 (2008).

28. Lundström, M., "Chalcopyrite dissolution in cupric chloride solutions", (2009).

29. Li, Y., Kawashima, N., Li, J., Chandra, A. P., and Gerson, A. R., "A review of the structure, and fundamental mechanisms and kinetics of the leaching of chalcopyrite", ***Advances In Colloid And Interface Science***, 197–198: 1–32 (2013).

30. Pradhan, N., Nathsarma, K. C., Srinivasa Rao, K., Sukla, L. B., and Mishra, B. K., "Heap bioleaching of chalcopyrite: A review", ***Minerals Engineering***, 21 (5): 355–365 (2008).

31. Prasad, S. and Pandey, B. D., "Alternative processes for treatment of chalcopyrite —A review", ***Minerals Engineering***, 11 (8): 763–781 (1998).

32. Yévenes, L. V., Miki, H., and Nicol, M., "The dissolution of chalcopyrite in chloride solutions: Part 2: Effect of various parameters on the rate", ***Hydrometallurgy***, 103 (1–4): 80–85 (2010).

33. Sokić, M. D., Marković, B., and Živković, D., "Kinetics of chalcopyrite leaching by sodium nitrate in sulphuric acid", ***Hydrometallurgy***, 95 (3–4): 273–279 (2009).

34. Dutrizac, J. E., "The dissolution of chalcopyrite in ferric sulfate and ferric chloride media", ***Metallurgical Transactions B***, 12 (2): 371–378 (1981).

35. Klauber, C., "A critical review of the surface chemistry of acidic ferric sulphate dissolution of chalcopyrite with regards to hindered dissolution", ***International Journal Of Mineral Processing***, 86 (1–4): 1–17 (2008).

36. Paynter, J. C., "A review of copper hydrometallurgy", ***Journal Of The Southern African Institute Of Mining And Metallurgy***, 74 (4): 158–172 (1973).

37. Fletcher, A. W., Sudderth, R. B., and Olafson, S. M., "Combining sulfate electrowinning with chloride leaching", ***JOM***, 43 (8): 57–59 (1991).

38. Baniasadi, M., Graves, J. E., Ray, D. A., De Silva, A. L., Renshaw, D., and Farnaud, S., "Closed-loop recycling of copper from waste printed circuit boards using bioleaching and electrowinning processes", ***Waste And Biomass Valorization***, 12 (6): 3125–3136 (2021).

39. Lundström, M., Aromaa, J., Forsén, O., Hyvärinen, O., and Barker, M. H., "Leaching of chalcopyrite in cupric chloride solution", ***Hydrometallurgy***, 77 (1): 89–95 (2005).

40. Wilson, J. P. and Fisher, W. W., "Cupric Chloride Leaching of Chalcopyrite", ***JOM***, 33 (2): 52–57 (1981).

41. Woodward, T., "On the operability of the Sherritt-Gordon ammonia leach at the Kwinana nickel refinery", PhD Thesis, ***Murdoch University***, (2014).

42. O'Connor, G. M. and Eksteen, J. J., "A critical review of the passivation and semiconductor mechanisms of chalcopyrite leaching", ***Minerals Engineering***, 154: 106401 (2020).

43. Shang, Y., Hasan, M. K., Ahammed, G. J., Li, M., Yin, H., and Zhou, J., "Applications of nanotechnology in plant growth and crop protection: a review", ***Molecules***, 24 (14): 2558 (2019).

44. Kirtane, A. R., Verma, M., Karandikar, P., Furin, J., Langer, R., and Traverso, G., "Nanotechnology approaches for global infectious diseases", ***Nature Nanotechnology***, 16 (4): 369–384 (2021).

45. Lowry, G. V., Avellan, A., and Gilbertson, L. M., "Opportunities and challenges for nanotechnology in the agri-tech revolution", ***Nature Nanotechnology***, 14 (6): 517–522 (2019).

46. Kim, K., Lee, J. K., Han, S. J., and Lee, S., "A novel top-down fabrication process for vertically-stacked silicon-nanowire array", ***Applied Sciences***, 10 (3): 1146 (2020).

47. Abid, N., Khan, A. M., Shujait, S., Chaudhary, K., Ikram, M., Imran, M., Haider, J., Khan, M., Khan, Q., and Maqbool, M., "Synthesis of nanomaterials using various top-down and bottom-up approaches, influencing factors, advantages, and disadvantages: A review", ***Advances In Colloid And Interface Science***, 102597 (2021).

48. Harano, K., "Self-assembly mechanism in nucleation processes of molecular crystalline materials", ***Bulletin Of The Chemical Society Of Japan***, 94 (2): 463–472 (2021).

49. Bag, S., Baksi, A., Wang, D., Kruk, R., Benel, C., Chellali, M. R., and Hahn, H., "Combination of pulsed laser ablation and inert gas condensation for the synthesis of nanostructured nanocrystalline, amorphous and composite materials", ***Nanoscale Advances***, 1 (11): 4513–4521 (2019).

50. Wack, S., Lunca Popa, P., Adjeroud, N., Vergne, C., and Leturcq, R., "Two-Step approach for conformal chemical vapor-phase deposition of ultra-thin conductive silver films", ***ACS Applied Materials & Interfaces***, 12 (32): 36329–36338 (2020).

51. Von Niessen, K., Gindrat, M., and Refke, A., "Vapor phase deposition using plasma spray-PVD^{TM}", ***Journal Of Thermal Spray Technology***, 19 (1): 502–509 (2010).

52. Mauer, G. and Vaßen, R., "Conditions for nucleation and growth in the substrate boundary layer at plasma spray-physical vapor deposition (PS-PVD)", ***Surface And Coatings Technology***, 371: 417–427 (2019).

53. Mattox, D. M., "Ion plating—past, present and future", ***Surface And Coatings Technology***, 133: 517–521 (2000).

54. Kelly, P. J. and Arnell, R. D., "Development of a novel structure zone model relating to the closed-field unbalanced magnetron sputtering system", ***Journal Of Vacuum Science & Technology A: Vacuum, Surfaces, And Films***, 16 (5): 2858–2869 (1998).

55. Ayuk, E. L., Ugwu, M. O., and Aronimo, S. B., "A review on synthetic methods of nanostructured materials", ***Chemistry Research Journal***, 2 (5): 97–123 (2017).

56. Le, H. A., Linh, L. T., Chin, S., and Jurng, J., "Photocatalytic degradation of methylene blue by a combination of TiO2-anatase and coconut shell activated carbon", ***Powder Technology***, 225: 167–175 (2012).

57. Schwander, M. and Partes, K., "A review of diamond synthesis by CVD processes", ***Diamond And Related Materials***, 20 (9): 1287–1301 (2011).

58. Ashfold, M. N., May, P. W., Petherbridge, J. R., Rosser, K. N., Smith, J. A., Mankelevich, Y. A., and Suetin, N. V., "Unravelling aspects of the gas phase chemistry involved in diamond chemical vapour deposition", ***Physical Chemistry Chemical Physics***, 3 (17): 3471–3485 (2001).

59. Dilger, S., Lizandara-Pueyo, C., Krumm, M., and Polarz, S., "Hierarchical Zinc Oxide Materials with Multiple Porosity Prepared by Ultrafast Temperature Gradient Chemical Gas-Phase Synthesis", ***Advanced Materials***, 24 (4): 543–548 (2012).

60. Schulz, C., Dreier, T., Fikri, M., and Wiggers, H., "Gas-phase synthesis of functional nanomaterials: Challenges to kinetics, diagnostics, and process development", ***Proceedings Of The Combustion Institute***, 37 (1): 83–108 (2019).

61. Cerda, J., Arbiol, J., Diaz, R., Dezanneau, G., and Morante, J. R., "Synthesis of perovskite-type BaSnO3 particles obtained by a new simple wet chemical route based on a sol–gel process", ***Materials Letters***, 56 (3): 131–136 (2002).

62. Ramesh, S., Natasha, A. N., Tan, C. Y., Bang, L. T., Niakan, A., Purbolaksono, J., Chandran, H., Ching, C. Y., and Teng, W. D., "Characteristics and properties of hydoxyapatite derived by sol–gel and wet chemical precipitation methods", ***Ceramics International***, 41 (9): 10434–10441 (2015).

63. Fan, J., Boettcher, S. W., and Stucky, G. D., "Nanoparticle Assembly of Ordered Multicomponent Mesostructured Metal Oxides via a Versatile Sol−Gel Process", ***Chemistry Of Materials***, 18 (26): 6391–6396 (2006).

64. Veith, M., Mathur, S., Lecerf, N., Huch, V., Decker, T., Beck, H. P., Eiser, W., and Haberkorn, R., "Sol-Gel Synthesis of Nano-Scaled BaTiO3, BaZrO3 and BaTi0.5Zr0.5O3 Oxides via Single-Source Alkoxide Precursors and Semi-Alkoxide Routes", ***Journal Of Sol-Gel Science And Technology***, 17 (2): 145–158 (2000).

65. Ge, S., Shi, X., Sun, K., Li, C., Uher, C., Baker Jr, J. R., Banaszak Holl, M. M., and Orr, B. G., "Facile hydrothermal synthesis of iron oxide nanoparticles with tunable magnetic properties", ***The Journal Of Physical Chemistry C***, 113 (31): 13593–13599 (2009).

66. Hayashi, H. and Hakuta, Y., "Hydrothermal synthesis of metal oxide nanoparticles in supercritical water", ***Materials***, 3 (7): 3794–3817 (2010).

67. Tulinski, M. and Jurczyk, M., "Nanomaterials Synthesis Methods", Metrology and Standardization of Nanotechnology, ***John Wiley & Sons, Ltd***, 75–98 (2017).

68. Asif, M. and Muneer, T., "Energy supply, its demand and security issues for developed and emerging economies", ***Renewable And Sustainable Energy Reviews***, 11 (7): 1388–1413 (2007).

69. Bradshaw, M. J., "Global energy dilemmas: a geographical perspective", ***The Geographical Journal***, 176 (4): 275–290 (2010).

70. Westerlund, S. and Ekstam, L., "Capacitor theory", ***IEEE Transactions On Dielectrics And Electrical Insulation***, 1 (5): 826–839 (1994).

71. Mojarad, S. A., Kwa, K. S., Goss, J. P., Zhou, Z., Ponon, N. K., Appleby, D. J., Al-Hamadany, R. A., and O'Neill, A., "A comprehensive study on the leakage current mechanisms of Pt/SrTiO3/Pt capacitor", ***Journal Of Applied Physics***, 111 (1): 014503 (2012).

72. Yanase, N., Abe, K., Fukushima, N., and Kawakubo, T., "Thickness dependence of ferroelectricity in heteroepitaxial BaTiO3 thin film capacitors", ***Japanese Journal Of Applied Physics***, 38 (9S): 5305 (1999).

73. Kim, B. C., Too, C. O., Kwon, J. S., Ko, J. M., and Wallace, G. G., "A flexible capacitor based on conducting polymer electrodes", ***Synthetic Metals***, 161 (11–12): 1130–1132 (2011).

74. He, Y., Zhang, Y., Li, X., Lv, Z., Wang, X., Liu, Z., and Huang, X., "Capacitive mechanism of oxygen functional groups on carbon surface in supercapacitors", ***Electrochimica Acta***, 282: 618–625 (2018).

75. Wu, Z., Li, L., Yan, J., and Zhang, X., "Materials Design and System Construction for Conventional and New-Concept Supercapacitors", ***Advanced Science***, 4 (6): 1600382 (2017).

76. Zhang, L., Hu, X., Wang, Z., Sun, F., and Dorrell, D. G., "A review of supercapacitor modeling, estimation, and applications: A control/management perspective", ***Renewable And Sustainable Energy Reviews***, 81: 1868–1878 (2018).

77. Rufer, A. and Barrade, P., "A supercapacitor-based energy-storage system for elevators with soft commutated interface", ***IEEE Transactions On Industry Applications***, 38 (5): 1151–1159 (2002).

78. González, A., Goikolea, E., Barrena, J. A., and Mysyk, R., "Review on supercapacitors: Technologies and materials", ***Renewable And Sustainable Energy Reviews***, 58: 1189–1206 (2016).

79. Elkholy, A. E., Heakal, F. E.-T., and Allam, N. K., "Nanostructured spinel manganese cobalt ferrite for high-performance supercapacitors", ***RSC Advances***, 7 (82): 51888–51895 (2017).

80. Raut, S. S. and Sankapal, B. R., "First report on synthesis of ZnFe2O4 thin film using successive ionic layer adsorption and reaction: approach towards solid-state symmetric supercapacitor device", ***Electrochimica Acta***, 198: 203–211 (2016).

81. Meher, S. K. and Rao, G. R., "Ultralayered Co3O4 for high-performance supercapacitor applications", ***The Journal Of Physical Chemistry C***, 115 (31): 15646–15654 (2011).

82. Deniz Turan, M., Boyrazlı, M., and Soner Altundoğan, H., "Improving of copper extraction from chalcopyrite by using NaCl", ***Journal Of Central South University***, 25 (1): 21–28 (2018).

83. Velásquez-Yévenes, L., Torres, D., and Toro, N., "Leaching of chalcopyrite ore agglomerated with high chloride concentration and high curing periods", ***Hydrometallurgy***, 181: 215–220 (2018).

84. Petrović, S. J., Bogdanović, G. D., and Antonijević, M. M., "Leaching of chalcopyrite with hydrogen peroxide in hydrochloric acid solution", ***Transactions Of Nonferrous Metals Society Of China***, 28 (7): 1444–1455 (2018).

85. Solís-Marcíal, O. J. and Lapidus, G. T., "Chalcopyrite leaching in alcoholic acid media", ***Hydrometallurgy***, 147–148: 54–58 (2014).

86. Pan, H., Yang, H., Tong, L., Zhong, C., and Zhao, Y., "Control method of chalcopyrite passivation in bioleaching", ***Transactions Of Nonferrous Metals Society Of China***, 22 (9): 2255–2260 (2012).

87. Hernández, P. C., Taboada, M. E., Herreros, O. O., Torres, C. M., and Ghorbani, Y., "Chalcopyrite dissolution using seawater-based acidic media in the presence of oxidants", ***Hydrometallurgy***, 157: 325–332 (2015).

88. Lu, J. and Dreisinger, D., "Copper leaching from chalcopyrite concentrate in Cu(II)/Fe(III) chloride system", ***Minerals Engineering***, 45: 185–190 (2013).

89. Turan, M. D. and Altundoğan, H. S., "Leaching of Chalcopyrite Concentrate with Hydrogen Peroxide and Sulfuric Acid in an Autoclave System", ***Metallurgical And Materials Transactions B***, 44 (4): 809–819 (2013).

90. Liddicoat, J. and Dreisinger, D., "Chloride leaching of chalcopyrite", ***Hydrometallurgy***, 89 (3): 323–331 (2007).

91. Saravanakumar, B., Ramachandran, S. P., Ravi, G., Ganesh, V., Guduru, R. K., and Yuvakkumar, R., "Electrochemical performances of monodispersed spherical CuFe2O4 nanoparticles for pseudocapacitive applications", ***Vacuum***, 168: 108798 (2019).

92. Wu, X., Wu, W., Li, Y., Li, F., and Liao, S., "Synthesis and electrochemical performance of rod-like CuFe2O4 as an anode material for Na-ion battery", ***Materials Letters***, 138: 192–195 (2015).

93. Polat, S. and Faris, D., "Fabrication of CuFe2O4@g-C3N4@GNPs nanocomposites as anode material for supercapacitor applications", ***Ceramics International***, 48 (17): 24609–24618 (2022).

94. Yang, X., Zhang, S., Yu, Q., Sun, P., Liu, F., Lu, H., Yan, X., Zhou, X., Liang, X., Gao, Y., and Lu, G., "Solvothermal synthesis of porous CuFe2O4 nanospheres for high performance acetone sensor", ***Sensors And Actuators B: Chemical***, 270: 538–544 (2018).

95. Guo, Y., Chen, Y., Hu, X., Yao, Y., and Li, Z., "Tween modified CuFe2O4 nanoparticles with enhanced supercapacitor performance", ***Colloids And Surfaces A: Physicochemical And Engineering Aspects***, 631: 127676 (2021).

96. Polat, S. and Mashrah, M., "Synthesis and electrochemical performance of MgFe2O4 with g-C3N4 on Ni-foam as composite anode material in supercapacitors", ***Journal Of Materials Science: Materials In Electronics***, 33 (30): 23427–23436 (2022).

97. Kongkaew, T. and Sakurai, K., "Low-temperature Synthesis of Cubic Phase CuFe2O4 Powder", ***Chemistry Letters***, 46 (10): 1493–1496 (2017).

98. Amir, Md., Gungunes, H., Slimani, Y., Tashkandi, N., El Sayed, H. S., Aldakheel, F., Sertkol, M., Sozeri, H., Manikandan, A., Ercan, I., and Baykal, A., "Mössbauer Studies and Magnetic Properties of Cubic CuFe2O4

Nanoparticles", ***Journal Of Superconductivity And Novel Magnetism***, 32 (3): 557–564 (2019).

99. Madhurambal, G. and Mariappan, M., "Growth and characterization of urea-thiourea non-linear optical organic mixed crystal", (2010).

100. Polat, S. and Faris, D., "Fabrication of CuFe2O4@g-C3N4@GNPs nanocomposites as anode material for supercapacitor applications", ***Ceramics International***, 48 (17): 24609–24618 (2022).

101. Zhang, R., Mao, Y., Liu, C., and Ni, W., "Synergistic catalytic effect of chloride ion and ammonium ion on the leaching of chalcopyrite in sulfuric acid solution", ***Minerals Engineering***, 185: 107686 (2022).

102. Mo, Y., Du, J., Lv, H., Zhang, Y., and Chen, A., "N-doped mesoporous carbon nanosheets for supercapacitors with high performance", ***Diamond And Related Materials***, 111: 108206 (2021).

103. Sharmila, V., Packiaraj, R., Nallamuthu, N., and Parthibavarman, M., "Fabrication of MWCNTs wrapped nickel manganese phosphate asymmetric capacitor as a supercapattery electrode for energy storage applications", ***Inorganic Chemistry Communications***, 121: 108194 (2020).

104. Polat, S., "Production of ZnFe2O4 Doped Carbon Cloth-Based Flexible Composite Electrodes for Supercapacitors", ***Türk Doğa Ve Fen Dergisi***, 10 (2): 199–205 (2021).

105. Ham, D., Chang, J., Pathan, S. H., Kim, W. Y., Mane, R. S., Pawar, B. N., Joo, O.-S., Chung, H., Yoon, M.-Y., and Han, S.-H., "Electrochemical capacitive properties of spray-pyrolyzed copper-ferrite thin films", ***Current Applied Physics***, 9 (1): S98–S100 (2009).

106. Zhao, J., Cheng, Y., Yan, X., Sun, D., Zhu, F., and Xue, Q., "Magnetic and electrochemical properties of CuFe 2 O 4 hollow fibers fabricated by simple electrospinning and direct annealing", ***CrystEngComm***, 14 (18): 5879–5885 (2012).

107. Niftaliyeva, A., Pehlivan, E., Polat, S., and Avci, A., "Chemical synthesis of single-layer graphene by using ball milling compared with NaBH4 and hydroquinone reductants", ***Micro & Nano Letters***, 13 (10): 1412–1416 (2018).

108. Polat, S., "Dielectric Properties of BN-ZnO-GNP Doped PU-EG Composites", ***International Journal Of Engineering Research And Development***, 13 (2): 635–644 (2021).

109. Polat, S., "Dielectric Properties of GNPs@MgO/CuO@PVDF Composite Films", ***Erciyes Üniversitesi Fen Bilimleri Enstitüsü Fen Bilimleri Dergisi***, 37 (3): 412–422 (2021).

110. Zhang, W., Quan, B., Lee, C., Park, S.-K., Li, X., Choi, E., Diao, G., and Piao, Y., "One-Step Facile Solvothermal Synthesis of Copper Ferrite–Graphene Composite as a High-Performance Supercapacitor Material", ***ACS Applied Materials & Interfaces***, 7 (4): 2404–2414 (2015).

111. Guo, Y., Chen, Y., Hu, X., Yao, Y., and Li, Z., "Tween modified CuFe2O4 nanoparticles with enhanced supercapacitor performance", ***Colloids And Surfaces A: Physicochemical And Engineering Aspects***, 631: 127676 (2021).

112. Zhu, M., Meng, D., Wang, C., and Diao, G., "Facile fabrication of hierarchically porous CuFe2O4 nanospheres with enhanced capacitance property", ***ACS Applied Materials & Interfaces***, 5 (13): 6030–6037 (2013)

.

RESUME

Mariem MOHAMED EL MAMY completed her primary, secondary and undergraduate education in Mauritania. She graduated from EL MAARIF School in Nouakchott in 2015 and started her education at UNIVERSITY OF NOUAKCHOTT ALASRIYA in the department of geology and graduated in 2019. In 2020 She started her education as a graduate student at Karabuk university (INSTITU OF APPLIED SCIENCE) Department of Metallurgy and material engineering.